

1 **Using flow cytometry and light-induced fluorescence technique to characterize the**
2 **variability and characteristics of bioaerosols in springtime at Metro Atlanta, Georgia**

3
4 Arnaldo Negron^{a,b}, Natasha DeLeon-Rodriguez^{c§}, Samantha M. Waters^{a#}, Luke D. Ziemba^d,
5 Bruce Anderson^d, Michael Bergin^e, Konstantinos T. Konstantinidis^{f,c*}, and Athanasios Nenes^{a,g,h*}

6 ^a School of Earth and Atmospheric Sciences, Georgia Institute of Technology, Atlanta, GA 30332, USA

7 ^b School of Chemical and Biomolecular Engineering, Georgia Institute of Technology, Atlanta, GA
8 30332, USA

9 ^c School of Biology, Georgia Institute of Technology, Atlanta, GA 30332, USA

10 ^d Chemistry and Dynamics Branch/Science Directorate, National Aeronautics and Space Administration
11 Langley Research Center, Hampton, VA 23681, USA

12 ^e Department of Civil and Environmental Engineering, Duke University, Durham, NC, 2770, USA

13 ^f School of Civil and Environmental Engineering, Georgia Institute of Technology, Atlanta, GA 30332,
14 USA

15 ^g Institute for Chemical Engineering Science, Foundation for Research and Technology Hellas, Patra,
16 GR-26504, Greece

17 ^h Laboratory of Atmospheric Processes and their Impacts (LAPI), School of Architecture, Civil &
18 Environmental Engineering, Ecole Polytechnique Fédérale de Lausanne, CH-1015, Switzerland

19 [§] Currently at: Puerto Rico Science, Technology and Research Trust, Rio Piedras, 00927, Puerto Rico

20 [#] Currently at: Department of Marine Sciences, University of Georgia, Athens, GA 30602-3636

21 ^{*}Corresponding Author

22 **Abstract**

23 The abundance and speciation of primary biological aerosol particles (PBAP) is important for
24 understanding their impacts on human health, cloud formation and ecosystems. Towards this, we have
25 developed a protocol for quantifying PBAP collected from large volumes of air with a portable wet-walled
26 cyclone bioaerosol sampler. A flow cytometry (FCM) protocol was then developed to quantify and
27 characterize the PBAP populations from the sampler, which were confirmed against epifluorescence
28 microscopy. The sampling system and FCM analysis were used to study PBAP in Atlanta, GA over a two-
29 month period and showed clearly defined populations of nucleic acid containing particles: Low Nucleic
30 Acid-content particles above threshold (LNA-AT), and High Nucleic Acid-content particles (HNA) likely
31 containing wet-ejected fungal spores, and pollen. We find that daily-average springtime PBAP
32 concentration (1 to 5 μ m diameter) ranged between 1.4×10^4 and 1.1×10^5 m⁻³. The LNA-AT population
33 dominated PBAP during dry days ($72 \pm 18\%$); HNA dominated the PBAP during humid days and following
34 rain events, where HNA comprised up to 92% of the PBAP number. Concurrent measurements with a
35 Wideband Integrated Bioaerosol Sensor (WIBS-4A) showed that FBAP and total FCM counts are similar;

36 HNA (from FCM) moderately correlated with ABC type FBAP concentrations throughout the sampling
37 period (and for the same particle size range, 1-5 μm diameter). However, the FCM LNA-AT population,
38 possibly containing bacterial cells, did not correlate with any FBAP type. The lack of correlation of any
39 WIBS FBAP type with the LNA-AT suggest airborne bacterial cells may be more difficult to
40 unambiguously detect with autofluorescence than currently thought. Identification of bacterial cells even in
41 the FCM (LNA-AT population) is challenging, given that the fluorescence level of stained cells at times
42 may be comparable to that seen from abiotic particles. HNA and ABC displayed highest concentration on
43 a humid and warm day after a rain event (4/14), suggesting that both populations correspond to wet-ejected
44 fungal spores. Overall, information from both instruments combined reveals a highly dynamic airborne
45 bioaerosol community over Atlanta, with a considerable presence of fungal spores during humid days, and
46 LNA-AT population dominating bioaerosol community during dry days.

47 **Introduction**

48 Primary biological aerosol particles (PBAP), also called bioaerosols, are comprised of airborne
49 microbial cells (e.g. bacteria, diatoms), reproductive entities (e.g. pollen, fungal spores), viruses and
50 biological fragments. Bioaerosols are ubiquitous, with potentially important impacts on human health,
51 cloud formation, precipitation, and biogeochemical cycles (Pöschl, 2005; Hoose et al., 2010; DeLeon-
52 Rodriguez et al., 2013; Morris et al., 2014; Longo et al., 2014; Fröhlich-Nowoisky et al., 2016;
53 Myriokefalitakis et al., 2016). Despite their low number concentration relative to abiotic particles, PBAP
54 possess unique functional and compositional characteristics that differentiate them from abiotic aerosol.
55 For example, certain PBAP constitute the most efficient of atmospheric ice nucleators, affecting the
56 microphysics of mixed phase clouds and precipitation (Hoose and Möhler, 2012; Sullivan et al., 2017). The
57 mass and nutrient content of PBAP may suffice to comprise an important supply of bioavailable P to
58 oligotrophic marine ecosystems (Longo et al., 2014; Myriokefalitakis et al., 2016). In addition, the
59 concurrence of disease outbreaks during dust storms has been attributed to pathogenic microbes attached
60 to airborne dust that are subsequently inhaled (Griffin et al., 2003; Ortiz-Martinez et al., 2015; Goudie
61 2014).

62 Quantification of the concentration and size of PBAP is critical for understanding their environmental
63 impacts. Measuring PBAP however poses a challenge for established microbiology tools, owing to their
64 low atmospheric concentration ($10^3 - 10^6$ cells m^{-3} air; Fröhlich-Nowoisky et al., 2016) and wide diversity
65 of airborne particle types and sizes. For instance, only a fraction of microorganisms (an estimated 5%; Chi
66 and Li et al., 2007) can be cultured, and cultivation cannot be used to quantify dead organisms, viruses or
67 fragments, while most culture-independent methods are optimized for more abundant microbial
68 populations. Epifluorescence microscopy (EPM) is the standard for bioaerosol quantification but is not

69 high-throughput and requires considerable time for quantification of concentration per sample. Flow
70 cytometry (FCM) is an analysis technique based on the concurrent measurement of light scattering and
71 fluorescence intensity from single particles (Wang et al., 2010). FCM requires a liquid suspension of
72 bioparticles that flows through an optical cell and interrogated with a series of laser beams. Each sample is
73 pretreated with stains that targeting specific macromolecules (e.g. DNA/RNA) which subsequently
74 fluoresce when excited by the FCM lasers. The resulting scattering and fluorescent light emissions are then
75 detected by an array of sensors to allow the differentiation of biological and abiotic (e.g. dust) particles
76 according to the characteristic specific to the stain used. FCM has proved to be as reliable as EPM, but with
77 the advantage of lower uncertainty, higher quantification efficiency and requiring considerably less time
78 and effort than EPM per sample (Lange et al., 1997). FCM is frequently used in biomedical research to
79 quantify eukaryotic cell populations, and in microbiology to quantify a wide variety of yeast and bacterial
80 cells (Nir et al., 1990; Van Dilla et al., 1983). FCM is also used to study environmental samples, e.g., to
81 differentiate low nucleic acid (LNA) from high nucleic acid (HNA) phytoplankton in aquatic environments
82 (Wang Y. et al 2010; Müller et al., 2010). Despite its advantages, FCM has seen little use in the bioaerosol
83 field to date, owing in part to the challenges associated with collecting sufficient PBAP mass for robust
84 counting statistics to be obtained (Chen and Li, 2005; Liang et al., 2013). Chen and Li (2005) determined
85 that for counting purposes, the SYTO-13 nucleic acid stain is the most effective (among five different
86 nucleic acid stains studied) for determining reliable concentration of bioaerosols.

87 Light Induced Fluorescence (LIF) is an increasingly utilized technique for bioaerosol quantification,
88 and it relies on measuring the autofluorescence intensity of specific high yield fluorophores (e.g.,
89 Nicotinamide Adenine Dinucleotide – NADH co-enzyme, flavins and amino acids like Tryptophan and
90 Tyrosine) present in PBAP. The major advantage of the technique is that it is fully automated, does not
91 require a liquid suspension (i.e., it directly senses particles suspended in air) and it provides high frequency
92 measurements (~1 Hz) make it ideal for continuous monitoring and operation in highly variable
93 environments (e.g., aircraft operation). Particles detected by LIF, called Fluorescent Biological Aerosol
94 Particles (FBAP), although not equal to PBAP, may still constitute a large fraction of the biological particles
95 (Healy et al., 2014; Gosselin et al., 2016). Using LIF, FBAP diurnal cycles showing maximum
96 concentrations during evenings and minimum around middays, especially in heavily vegetated
97 environments have been observed. This behavior has been related to known temperature and relative
98 humidity release mechanism of certain fungal spore species (Wu et al., 2007; Gabey et al., 2010; Tropak
99 and Schnaiter, 2013). Huffman et al. (2010) used a UV-Aerodynamic Particle Sizer (UV-APS) to show that
100 the concentration and frequency of occurrence of 3µm FBAP particles at Mainz, Germany (semi-urban
101 environment) exhibited a strong diurnal cycle from August through November: with a first peak at ~
102 $1.6 \times 10^4 \text{ m}^{-3}$ at mid-morning (6-8 am) followed by a constant profile ($\sim 2\text{-}4 \times 10^4 \text{ m}^{-3}$) throughout the rest of

103 the day. Similar studies in urban and densely vegetated environments suggest a notable difference in the
104 size distributions, diurnal behavior and FBAP loading between the two environments. Gabey et al., 2011
105 found that the FBAP in Manchester, UK follow a characteristic bimodal distribution with peaks at 1.2 μm
106 and 1.5 – 3.0 μm . As in Mainz, the concentration of larger particles peaks in the mid-morning, ranges from
107 0 to 300 L^{-1} , and the 1.2 μm peak is linked to traffic activity. However, at the Borneo tropical rain forest
108 FBAP concentrations peak during the evening with a robust 2-3 μm population and concentrations ranging
109 from 100 to 2000 L^{-1} (Gabey et al., 2010).

110 LIF-based observations (e.g. UV-APS, WIBS), combined with measurements of molecular tracers (e.g.
111 mannitol and arabitol) and endotoxin measurements provide a more complete picture of PBAP emissions.
112 Gosselin et al. (2016) applied this approach during the BEACHON-RoMBAS field campaign. A clear
113 correlation between FBAP and the molecular markers is seen, indicating an increase of fungal spores during
114 rain events. FBAP concentrations and molecular marker-inferred (arabitol and mannitol; Bauer et al., 2008
115 approach) fungal spore concentrations were within the same order of magnitude. WIBS-3 cluster
116 (determined using Crawford et al., 2015) linked to fungal spores gave concentrations 13% lower than those
117 derived from molecular marker concentrations during rain events. During dry events, FBAP and molecular
118 markers derived fungal spore concentrations were poorly correlated. It is currently unknown the degree to
119 which all types of PBAP are consistently detected by LIF over different time of the year and different
120 environments; it is likely, however, that for certain classes of bioparticles (e.g., pollen and fungi) the
121 detection efficiency using LIF is relatively high. However, the low intrinsic fluorescence intensity of
122 bacteria and high variability of thereof in relation to metabolic state may lead to their misclassification as
123 non-biological particles (Hernandez et al., 2016).

124 For LIF-based quantification of PBAP to be effective, it requires the intrinsic fluorescence of biological
125 material to exceed that of non-biological matter. Depending on the type, metabolic state and species, PBAP
126 autofluorescence may vary orders of magnitude and therefore LIF may not always be able to differentiate
127 between biological and abiotic particles. For example, Tropak and Schnaiter (2013) showed that laboratory-
128 generated mineral dust, soot and ammonium sulfate may be misclassified as FBAP. To address
129 misclassification, Excitation Emission Matrices (EEMs) have been developed for biomolecules (e.g.
130 tryptophan, tyrosine, riboflavin) and non-biological (e.g. Pyrene, Naphthalene, Humic Acid) molecules.
131 EEMs provide the wavelength-dependent fluorescence emission spectra as a function of the excitation
132 wavelength and are used to assign spectral modes to known fluorophores. The structure of EEMs is
133 important for identifying molecules that are unique to PBAP and allow their identification by LIF; it is this
134 principle upon which detectors in commercial FBAP measurements (e.g. WIBS, UV-APS) are based upon.
135 Comparison of EEMs from biological and non-biological molecules show that even when biomolecules

136 have higher autofluorescence intensity than non-biologicals in the LIF detection range, interferences from
137 non-biological compounds (e.g. polycyclic aromatic hydrocarbons and soot) from combustion emissions
138 can influence LIF detection (Pöhlker et al., 2012). Considerable work remains on determining which
139 detector(s) or combination thereof provides an unambiguous identification of bioaerosols and related
140 subgroups (e.g. bacteria, fungal spores, pollen). Towards this, an aerobiology catalog of pure cultures has
141 been developed for the WIBS-4 showing that instrument-to-instrument variability in fluorescence detection
142 poses a considerable challenge, as applying common detection thresholds across instruments leads to
143 considerable differences in PBAP concentration and composition (Hernandez et al., 2016).

144 Another important issue for LIF-based quantification of PBAP is the impact of atmospheric oxidants,
145 UV and other stressors on the fluorescence intensity of PBAP. Pan et al. (2014) tested the effect of relative
146 humidity and ozone exposure in the autofluorescence spectra of octapeptide aerosol particles using an UV-
147 APS connected to a rotating drum. Octapeptides, organic molecules containing eight amino acids and
148 present in cells, were used as a proxy to study the aging of tryptophan and results suggest bioaerosols
149 exposure to high, but atmospherically-relevant levels of ozone (~150ppb) decreases tryptophan
150 fluorescence intensity and PBAP detection. Multiple stressors can be affecting bioaerosols LIF detection
151 so such issues need to be thoroughly explored to understand PBAP detection efficiency over the wide range
152 of atmospheric conditions and PBAP population composition (Toprak and Schnaiter, 2013; Hernandez et
153 al., 2016).

154 The aims of the study are to (i) develop an effective and reliable FCM detection and quantification
155 protocol for bioaerosol; (ii) apply the protocol to understand bioaerosol populations and their variability
156 during different meteorological conditions, and, (iii) compare FCM and WIBS-4A results to have a better
157 understanding of PBAP day-to-day variability. To our knowledge, this study is the first to develop a FCM
158 protocol to identify and quantify well-defined speciated bioaerosols populations from samples collected
159 from a modified state-of-the-art biosampler. LIF sampling of bioaerosol side-by-side with established and
160 quantitative biology tools (FCM and EPM) was conducted to assess the LIF detection capabilities toward
161 different bioaerosol populations and under atmospherically-relevant conditions during this study. Atlanta
162 is selected as a case study for PBAP sampling, as it provides a highly populated urban environment
163 surrounded by vast vegetative areas; this and the broad range of temperature and humidity ensures a wide
164 range of PBAP population composition, state and concentrations. All the samples collected are compared
165 side-by-side to concurrent WIBS-4A data collected over the same time period.

166

167

168

169 **2. Instrumentation and Methodology**

170 **2.1 Bioaerosol Sampler**

171 Sampling was performed using the SpinCon II (InnovaPrep LLC, Inc.) portable wet-walled cyclone
172 aerosol sampler. Aerosol is collected by inertial impaction with a recirculating liquid film in the cyclone;
173 evaporative losses are compensated so that the sample volume is maintained constant during a sample cycle.
174 The particle collection efficiency for 1 μ m, 3 μ m, 3.5 μ m and 5.0 μ m particles is about 47.3 \pm 2.1%,
175 56.1 \pm 3.9%, 14.6 \pm 0.6 and 13.8 \pm 2.2%, respectively (Kesavan et al., 2015). However, the experiments
176 conducted using 1 μ m PSL and 3 μ m PSL, 3.5 μ m oleic acid and 5.0 μ m oleic acid particles not necessarily
177 quantify the collection efficiency of biological particles in this size range. Even with a lower collection
178 efficiency than any impingement sampler, SpinCon effectively collects larger amounts of biological
179 particles owing to its high volumetric flow rate, which is a considerable advantage (Kesavan et al., 2015).
180 However, the stress caused by the high flow rate of the SpinCon may affect cell viability. Santl-Temkiv et
181 al. (2017) recently studied the SpinCon retention efficiency from sea water samples and for *P.agglomerans*
182 populations from pure cultures ($\sim 10^5$ cells mL⁻¹). After 1 hour of sampling, the SpinCon was found to
183 retain 20.6 \pm 5.8% of the *P.agglomerans* concentration and 55.3 \pm 2.1% of the sea water microbial
184 concentration.

185 In our study, the biosampler was run at 478L min⁻¹ for 4hr sampling cycles. Phosphate-buffered saline
186 (PBS) 1X pH 7.4 solution was used and the instrument compensated for water evaporation by supplying
187 Milli-Q water to maintain the PBS concentration constant. Upon termination of each sampling cycle, the
188 instrument was programmed to dispense the sample in a 15mL centrifuge tube. Then, 10 μ l of formalin (37
189 wt.% formaldehyde) per mL of solution was added to every sample for preservation and samples were
190 stored at 4°C. Given the long sampling times and the low concentration of PBAP, the fluid supply system
191 of the instrument was modified and a cleaning protocol (CP) has been developed, which is described below.

192 The SpinCon II water and PBS supply bags used in the commercial instrument were replaced by two
193 2L autoclavable Nalgene bottles (Thermo Scientific Inc.) with antimicrobial tubing, connectors and a small
194 HEPA filter connected to vent and prevent coarse and submicron particles contamination (Figure 1). Bottles
195 were autoclaved and filled with Milli-Q water and PBS, beforehand sterilized with 0.2 μ m pore bottle top
196 filters (Thermo Fisher Inc.) and transferred inside a biosafety cabinet. An aliquot of each fluid obtained
197 after preparation was evaluated for sterility by EPM and FCM.

198 The cleaning protocol (CP) of the biosampling system consists of two phases. During phase one, all
199 acrylic windows and the outside of the collector/concentrator were cleaned with ethanol 70 wt. %. Then,
200 the instrument inlet, outlet, and the inside of the collector/concentrator was cleaned with ethanol 70 wt. %.

201 In the second phase, the SpinCon II inlet was connected to a HEPA filter to provide a particle-free source
202 of air to the sampling system; the instrument was then washed with ethanol 70 wt.%, 10 wt.% bleach
203 solution, PBS and Milli-Q H₂O, respectively. The wash consisted of a rinse, a 2 minutes sample and filling
204 the instrument collector/concentrator with the fluid in use (i.e., bleach solution, ethanol, PBS and Milli-Q
205 H₂O). The collector/concentrator was drained after 1 minute. The above were repeated for the remaining
206 fluids, taking 5 minutes per fluid. Overall, the CP requires 45 minutes; upon completion, a blank is obtained
207 to constrain the residual contamination levels after cleaning (described below). Finally, the HEPA filter
208 was disconnected, instrument inlets and outlets were sealed and the inlet tube was cleaned with ethanol 70
209 wt.% to be ready for rooftop sampling. SpinCon II was rinsed with ethanol 70wt.% after each sampling
210 episode and the cleaning protocol was applied before each sample.

211 Several blanks were obtained to quantify the levels of PBAP contamination in the fluids and sampler,
212 and to ensure that they were sufficiently low to not bias the detection, identification and quantification of
213 the PBAP. Furthermore, an instrument blank was obtained after a CP to constrain residual particles, by
214 running the sampler for 2 minutes, while sampling air with a HEPA filter connected to the inlet of the
215 SpinCon II. Another blank was collected to characterize any contamination of biological particles from the
216 supply of PBS and water in the SpinCon II. This was done by operating the SpinCon II for a 4hr period
217 with a HEPA filter connected to the inlet which completely cleans the air entering the wet cyclone from
218 any bioparticles. All blanks were analyzed directly via FCM (Sect. 2.3) and EPM.

219 The volumetric flow rate within the SpinCon II was routinely calibrated by a VT100 Hotwire Thermo-
220 anemometer (Cole Palmer Inc.) using a 3-hole round duct transverse approach. A 1 ¼" OD tube with the
221 same diameter as the SpinCon II inlet was designed with 3 holes. Each hole was 60° apart from the other
222 and the holes were perpendicular to the axial air flow direction of the tube. (Supplementary Information,
223 Figure S1). Triplicates of flow rate measurements were taken in each hole at the center of the tube and
224 averaged to determine SpinCon II volumetric flow rate ($478.0 \pm 6.4 \text{ L min}^{-1}$).

225 **2.2 Flow Cytometry**

226 During this study, a BD Accuri C6 flow cytometer (BD Bioscience Inc.) was used for Flow Cytometry.
227 The instrument quantifies suspended cells in aqueous medium at three flow velocity modes (slow, medium
228 and fast flow at 14, 35 and 66 $\mu\text{L min}^{-1}$, respectively). It excites particles with a 488nm laser and possesses
229 four fluorescence detectors: FL1 (533±30nm), FL2 (585±40nm), FL3 (> 670nm) and FL4 (675±25nm),
230 which make it possible to analyze the fluorescence from multiple dyes concurrently. In this study, 2.5 μM
231 SYTO-13 nucleic acid probe was added to the fixed samples and incubated for 15min in the dark at room
232 temperature to stain biological particles. Additionally, 10 μL of 15 μm polystyrene bead suspension was
233 added to the 1mL total volume samples as an internal standard for PBAP concentration and size

234 quantification. The BD Accuri C6 was cleansed before each use with 0.2 μ m filtered Milli-Q water in fast
235 mode for 10min; background particle counts were typically reduced to 1 μ L⁻¹. At the beginning of every
236 experiment, a 1mL blank of the atmospheric sample without SYTO-13 and beads was analyzed, used in
237 quantification calculations (Sect. 3.1). Each sample was run in slow mode for 5min. After each sample, the
238 instrument was flushed with 0.2 μ m filtered Milli-Q water in slow flow for 1 minute (important for robust
239 quantification of the typically low concentrations of the atmospheric samples). SYTO-13 fluorescence
240 intensity was quantified by the FL1-A detector and used in combination with other parameters (FSC-A &
241 SSC-A) to constrain the PBAP populations present. FSC-A measured forward ($0^\circ \pm 13^\circ$) scattering and is
242 used to characterize the size of particles; SSC-A measured the side ($90^\circ \pm 13^\circ$) scattering and is used to
243 characterize the internal complexity of particles. The SSC-A scattering intensity is a function of the cellular
244 granularity or density of the internal structures (e.g. nucleus, mitochondria, ribosomes), the sphericity and
245 size of the particles. Compared to spherical particles of the same size, elongated particles tend to yield a
246 broader distribution of side scattering intensities (Mage et al., 2019; Mathaes et al., 2013). Although side
247 scattering intensity increases with particle size, it has not been commonly used to measure cell size (Tzur
248 et al., 2011). Overall, SSC-A scattering intensity will be proportional to the amount scattering caused by
249 the internal structures and the cell membrane, which ultimately depends on the refractive index of each cell
250 (Muller et al., 2010). Side scattering has been effective to distinguish cells of different complexities (e.g.
251 monocytes and granulocytes; Shapiro, 2005).

252 A 80,000 unit intensity FSC-H threshold (default FSC-H threshold value suggested by the manufacturer
253 to minimize the effect of noise) was set in the instrument during data acquisition to minimize the effects of
254 noise on bioparticle counts. The FSC-H channel (where H denotes height), measures single-particle forward
255 scattering (FSC) intensity based on the peak (maximum point) of the voltage pulse curve recorded when a
256 single particle goes through the interrogation point in the flow cytometer, whereas FSC-A, where A denotes
257 area, measures single-particle FSC intensity based on the area below the curve of the recorder pulse. When
258 the 80,000 unit FSC-H threshold is defined, only signals with an intensity greater than or equal to threshold
259 value will be processed, and this could affect the statistics and detection efficiency of the flow cytometer
260 toward small particles ($\leq 1\mu$ m). Experiments conducted with 1.0 μ m polystyrene beads suspension
261 (Supplemental information; Figure S16) have shown that 1.0 μ m beads have FSC-H intensities above the
262 80k threshold, no particle losses is observed, and beads estimated concentration agree with the reported by
263 the manufacturer ($\sim 6 \times 10^7$ mL⁻¹; Life Technologies, Inc.) The FCM data from each sample was analyzed
264 using the Flow Jo software (<https://www.flowjo.com/solutions/flowjo>) to gate and quantify bioparticles
265 population. The same procedure was used to analyze the PBS, Milli-Q water and blanks.

266

267 2.3 LIF detection of PBAP

268 The WIBS-4A (referred to henceforth as “WIBS”) is a single biological particle real time sensor, which
269 measures particle light scattering and autofluorescence in an approximately 0.5 – 15µm particle range
270 (www.dropletmeasurement.com). Particles are initially sized using the 90-degree side-scattering signal
271 from a 635 nm continuous-wave diode laser. The scattering intensity is directly related to particle diameter
272 and was calibrated prior to deployment using polystyrene latex sphere calibration standards (PSL with 0.8,
273 0.9, 1.0, 1.3, 2.0, 3.0 µm diameter, Thermo Scientific Inc.). The WIBS optical size therefore refers to PSL
274 material with a real refractive index of 1.59. Healy et al. (2012) determined WIBS-4 counting efficiency by
275 aerosolizing standardized concentrations of PSL sphere of specific sizes (e.g. 0.3, 0.4, 0.56, 0.7, 0.9 and
276 1.3µm) and compared WIBS-4 total counts against PSL counts detected by the condensation particle
277 counter (CPC). Results show WIBS-4 possesses a 50% counting efficiency for 0.5µm particles and detects
278 100% of the PSL particles above 0.7µm when it is compared to the CPC counts. The 280nm and 370nm
279 pulsed Xenon flashtube UV lights in the WIBS cause the particles to autofluoresce (i.e., excite the
280 chromophores preexisting in the PBAP and do not rely on a fluorescent dye as done in FCM). Then,
281 fluorescent emissions are measured at three wavelength channels, which following the nomenclature of
282 Perring et al. (2015) are: (i) channel A (“FL1_280” in previous studies; Robinson et al., 2013), which refers
283 to the detected emission between 310-400nm after excitation at 280nm, (ii) channel B (“FL2_280” in
284 previous studies), which refers to the detected emission between 420-650nm after excitation at 280nm, and,
285 (iii) channel C (“FL2_370” in previous studies), which refers to the detected emission between 420-650nm
286 after excitation at 370nm. The resulting autofluorescence from 280nm excitation is affected by the presence
287 of tryptophan, tyrosine and phenylalanine amino acids in the PBAP (Pöhlker et al., 2012). Similarly, the
288 resulting autofluorescence from the 370nm excitation is influenced by the presence of riboflavin and co-
289 enzyme Nicotinamide Adenine Dinucleotide Phosphate (NAD(P)H) within the cells.

290 Biological and non-biological particles can be discriminated by using a fluorescent intensity threshold;
291 here the threshold is determined with the Gabey et al. (2010) method and with modifications by Perring et
292 al. (2015) as follows. Particles with fluorescence intensities below the fluorescence threshold in all channels
293 are categorized as non-fluorescent (NON-FBAP). Particles that fluoresce above the threshold in only one
294 channel are named with a single letter (e.g. A, B or C); particles that fluoresce in two channels are named
295 with the two channel letters (e.g. AB, AC or BC), while particles that fluoresce in all channels are
296 categorized as type ABC. Furthermore, the total FBAP concentration is defined as the sum of the
297 concentration in the seven FBAP categories defined above. This approach was applied by Hernandez et al.,
298 (2016) to pure culture PBAP (bacteria, fungal spores, pollen) to study their correspondence to FBAP types;
299 bacteria tend to be detected by type A, and fungal spores and pollen by type AB and ABC. However,
300 bioaerosol classification is instrument-specific and particle size dependent (Hernandez et al., 2016; Savage

301 et al., 2017). Multiple environments have been studied using the Perring et al. 2015 FBAP types, including
302 rural, urban and highly vegetated locations. In the Southeastern US, the total FBAP concentration range
303 from 2×10^4 to $8 \times 10^4 \text{ m}^{-3}$, constituting 3-24% of the total supermicron particle number between 1 and $10 \mu\text{m}$
304 diameter. In the highly vegetated Rocky Mountains, ABC type particles are enhanced during rainy days
305 (during or post-rain events) to $\sim 65\%$ of the total FBAP, owing to the release of wet-ejected fungal spores
306 following precipitation (Gosselin et al., 2016). On the contrary, in the highly populated city of Nanjing,
307 China all FBAP types, except type C, correlated with black carbon concentrations, suggesting a strong
308 interference by combustion sources (Yu et al., 2016). A detailed explanation of the above-mentioned studies
309 using Perring et al. 2015 approach is also included in the section SI.20 of the supplemental information.

310 **2.4 Location of sampling site and sampling frequency**

311 Bioaerosol sampling was conducted between April 7 and May 15, 2015 at the rooftop sampling
312 platform of the Ford Environmental Sciences and Technology (ES&T) building at the Georgia Institute of
313 Technology campus in Atlanta, GA. The site, which was located at the heart of a major urban environment,
314 is surrounded by dense forested areas in the southeastern USA: the Oconee National Forest (South East),
315 the Chattahoochee National Forest (North), and the Talladega National Forest (West). The WIBS was
316 operating continuously throughout the same period, sampling bioaerosol from a 15 ft. long and $\frac{1}{4}$ in. ID
317 conductive tubing inlet fixed 8 ft. above the sampling platform floor. The SpinCon II was placed in the
318 platform during sampling episodes with its inlet facing South. Three 4-hour samples per week were
319 collected with the Spincon II sampler over the 5-week period (4 h sampling between 10am and 5pm; Table
320 1). Meteorological data acquired from the same platform provided wind speed, wind direction, relative
321 humidity (RH), temperature, total hourly rain and UV radiation index with a 1min resolution.

322 **3. Data processing and Analysis**

323 **3.1 FCM data processing**

324 All blanks collected showed contamination levels that did not exceed 1% of the PBAP quantified in the
325 subsequent atmospheric samples. The 2-minute instrument blanks obtained after the CP and the HEPA filter
326 washes was $1.06 \times 10^3 \pm 7.37 \times 10^2 \text{ mL}^{-1}$ and $9.22 \times 10^2 \pm 1.24 \times 10^2 \text{ mL}^{-1}$, respectively, which are negligible
327 accumulations compared to the $2.55 \times 10^5 \pm 1.14 \times 10^5 \text{ mL}^{-1}$ average PBAP concentration quantified in the
328 atmospheric samples. The concentration of PBAP in the blanks was also confirmed with microscopy (not
329 shown). Based on this, we are confident that the CP protocol and procedure to replace the working fluids
330 ensured sterility of the biosampler before each sampling.

331 FCM analysis of the samples was carried out as follows. We obtain the fluorescence intensity (from
332 each of the 4 fluorescence detectors), forward scattering and side scattering intensity for all the particles
333 suspended in the samples. A gating procedure was used to determine the fluorescence levels associated

334 with detecting only particles containing SYTO-13 (hence, a PBAP) and background fluorescence from non-
335 stained particles. The procedure (Supplemental information, SI.2 and SI.3) consists of 3 steps: (a)
336 fluorescence threshold determination, (b) population gating, and, (c) biological/non-biological particle
337 discrimination in the population(s) within the threshold (e.g. LNA PBAP, Section 4.1). The fluorescence
338 threshold was determined using an atmospheric sample without SYTO-13 collected before each FCM
339 analysis, as a blank. Based on the fluorescence responses obtained, we determine the FL1-A fluorescence
340 intensity value for which 99.5% or 99.9% of the (unstained) particles of the blank autofluoresce below the
341 chosen value. This FL1-A intensity, called “fluorescence threshold”, was determined for each sample
342 (supplementary information, Figure S2a and S2b). The determination of the fluorescence threshold
343 involved selecting the most conservative value that maximizes inclusion of biological particles and
344 minimizes the inclusion of non-biological particles, including those that may be subject to background
345 fluorescence or unspecific binding of SYTO-13 (Diaz et al., 2010; Müller et al., 2010). We found out that
346 threshold values for the 99.9% approach were substantially higher than 99.5% approach in multiple
347 sampling events and comparable to the fluorescence intensities observed for stained pure cultures ($\sim 10^5$
348 units), which means that the 99.9% threshold values will miscount pure cultures as non-biological.
349 Consequently, we set the fluorescence threshold to the highest fluorescence intensity value observed by the
350 99.5% approach (41,839 units; supplementary information, Figure S2b), applied it to all collected samples;
351 henceforth named the 42k FL1-A threshold. The 42k threshold value aims to minimize any abiotic
352 interference as it maximizes biological particles quantification. A fixed value has been chosen and applied
353 to all samples given that having a different threshold value for each sampling event may result in
354 quantification biases as bioaerosols with strong autofluorescence (e.g. pollen, fungal spores) can increase
355 the threshold value and affect PBAP quantification in the population(s) within the threshold. The BD Accuri
356 C6 flow cytometer used for the analysis of the samples maintains constant pre-optimized photomultiplier
357 voltages and amplifier gain settings. As a result, the fluorescence intensity of particles is consistent from
358 day-to-day, and the fluorescence intensity of a specific biological particle population having the same
359 metabolic state and physiological characteristics must not show day-to-day variability
360 (www.bdbiosciences.com). Under the 42k threshold approach PBAP concentrations in the population(s)
361 within the threshold (e.g. LNA, Section 4.1) can be overestimated by up to a 0.5%. Furthermore, FCM
362 experiments conducted with unprocessed Arizona Test Dust (ATD) show that the FL1_A intensity
363 distribution of SYTO-13 stained ATD particles is very similar to unstained ATD particles, and 100% of the
364 SYTO-13 stained ATD particles stay below the 42k threshold (supplementary information, Figure S14a and
365 S14b), supporting the 42k threshold effectiveness to filter out abiotic particles.

366 Once the FL1-A threshold was determined, plots of FL1-A vs. SSC-A and FL1-A vs. FSC-A are used
367 to define clusters of bioparticles with fluorescence that exceed the FL1-A threshold and a characteristic

368 optical size (obtained from the FSC-A intensity) or particle internal complexity (obtained from the SSC-A
369 intensity). FL1-A vs. SSC-A plots were used to define the populations of bioparticles for PBAP
370 quantification as clusters using SSC-A parameter were more defined and showed better spatial resolution
371 than using FSC-A parameter. The limits of each population were also determined with Flow Jo
372 (www.flowjo.com), using 2% contour plots (supplemental information; Figure S3) generated by equal
373 probability contouring (i.e., 50 contour levels so that the same number of cells fall between each pair of
374 contour lines). Populations above the FL1-A threshold value (41,839 FL1-A units) were considered
375 biological (Section 4.1; e.g. HNA); the particles in the population within the threshold value (Section 4.1;
376 e.g. LNA) having a FL1-A intensity greater than 41,839 units were counted as biological to determine the
377 PBAP counts in the population. The total PBAP counts were considered as all particles counts having FL1-
378 A fluorescence intensity above the determined threshold value minus the 15 μ m beads internal standard
379 having FL1-A fluorescence intensity above the determined threshold value. The 15 μ m beads of known
380 concentration and particle size allows for calibrating the optical size (supporting information, SI.7) of the
381 bioparticles, as well as their concentration and departure from sphericity. The 15 μ m beads population
382 showed fluorescence intensities comparable to the determined fluorescence threshold after been stained
383 with SYTO-13 as it is known that molecular stains can be adsorbed on the surface of polystyrene beads
384 (Eckenrode et al., 2005; Rödiger et al., 2011). The relatively high fluorescence intensity of the 15 μ m beads
385 show populations within the threshold value (e.g. LNA, Section 4.1) cannot be rule out as being affected
386 by unspecific staining of abiotic particles. However, populations above the threshold value (e.g. HNA,
387 Section 4.1) should not be affected by such abiotic interferences.

388 **3.2 WIBS data processing**

389 15-minute average total aerosol and FBAP size distributions were obtained from the WIBS. FBAP was
390 distinguished from the total aerosol using the Gabey et al. (2010) “trigger threshold” approach, which is
391 applied as follows. First, the average “electronic fluorescence noise” and its standard deviation is
392 determined for each channel (A, B, C) performing the Force Trigger (FT) calibration which consist to
393 operate the WIBS without flowing air through the system. The FT calibration, carried out every 24hr, is
394 critical for determining the lowest particle autofluorescence levels that robustly exceeds instrument
395 electronic noise. FT calibrations measured the particle-free air background autofluorescence in the three
396 WIBS channels (e.g. A, B, C), and measurements recorded the fluorescence intensity for 500 excitation
397 flash events (Ziemba et al., 2016; Tropak and Schnaiter, 2013; Gabey et al., 2010). The threshold for each
398 detector is then equal to the average fluorescence plus 2.5 times its standard deviation; particles with
399 fluorescence intensities above this threshold value are classified as FBAP. Then, Perring et al. (2015)
400 approach (Section 2.3) is applied to determine the combination of thresholds that provide the maximum
401 concentration of PBAP and minimal interference from abiotic particles, which still remains an area of active

402 research. It is important to note that the Gabey et al. (2010) threshold approach and the Perring et al. (2015)
403 FBAP types were applied to the WBS-4A data and should not be directly compared to FBAP
404 quantifications performed by the WBS-3 in previous studies, owing to the channel A and B overlap on the
405 latter. A detailed comparison between WBS-3 and WBS-4 models, as well as PBAP detection by both
406 models, is further discussed in the supplemental information (SI.20).

407 In this study, thresholds for each channel were determined daily, and the total particle concentration,
408 FBAP types (e.g. A, B, C, AB, BC, AC, ABC) concentrations and the total FBAP concentration (sum of
409 the seven FBAP types) were used. From the data, 4h-averaged size distributions (using 15-minute average
410 data) were generated for the total particles and all FBAP types in the 1-10 μ m range during the time SpinCon
411 II run. Subsequently, WBS overall sampling efficiency (aspiration efficiency + transport efficiency) was
412 calculated using the Particle Losses Calculator (Von der Weiden et al., 2009) and applied to the 1-10 μ m
413 size distributions for the sampling characteristics in our setup (15ft. sampling line with ¼ in. ID and 2.3 L
414 min⁻¹ flow rate; Figure S4a). The sampling efficiency was calculated to be 67% for 5 μ m particles, with
415 larger losses as size increased to 10 μ m. (supplemental information, FigureS4b). FCM and WBS total
416 particles and PBAP comparison was constrained to the 1 to 5 μ m range being the size overlap of both
417 techniques. Also, the fractional composition of FBAP (based on number concentrations) was calculated to
418 characterize its daily variability (Section 4.2), and compared against the daily variability of PBAP from the
419 FCM analysis (Section 4.4).

420 **4. Results and Discussion**

421 **4.1 FCM biopopulation identification and quantification**

422 When the FCM results are plotted in terms of FL1-A fluorescence intensity versus SSC-A scattering
423 intensity, four populations (Figure 2) emerge above the detection thresholds: low nucleic acid (LNA)
424 particles, high nucleic acid (HNA) particles, pollen and the 15 μ m internal standard beads. EPM and SEM
425 pictures (Supplementary Figures S5, S6, and S7) confirm the presence of these heterogeneous populations.
426 SYTO-13 stains DNA and RNA, and the resulting single-cell FL1-A fluorescence intensity (Figure 2) is
427 directly proportional to its nucleic acid content (Lebaron et al.,2001; Troussellier et al.,1999; Comas-Riu et
428 al., 2002). Previously, SYTO-13 has effectively distinguish between HNA and LNA bacterioplankton and
429 phytoplankton populations in fresh and seawater samples, and results are comparable to SYBR green II and
430 SYBR green I, more specific DNA probes (Wang et al., 2010; Bouvier et al., 2007; Lebaron et al., 2001).
431 However, corresponding populations in atmospheric PBAP have not been identified before. The SSC-A
432 scattering intensity in Figure 2 changes as function of size, composition (e.g. cell refractive index) and
433 complexity of the cell (e.g. internal structures or surface irregularities), and the strongest SSC-A intensity

434 corresponding to the largest, most complex particles. Below we focus on each population to further
435 understand the identified populations of biological particles.

436 The HNA size distributions are dominated by 3-5 μm particles (mean diameter: $4.15 \pm 0.06 \mu\text{m}$;
437 Supplemental Information, Figure S10) and the total concentration moderately correlated with RH. HNA
438 were virtually non-existent during several extended dry periods (days with average RH < 70% during
439 sampling, e.g. 4/9, 4/22 and 5/15) and well defined during periods of high humidity, especially after rain
440 events (days with average RH > 70% and T > 18 °C during sampling episode; e.g. 4/7, 4/14, 4/15). Both of
441 these characteristics suggest that HNA particles correspond to wet-ejected fungal spores (e.g., from the
442 Ascospores and Basidiospores genus; Oliveira et al., 2009; Li and Kendrick, 1995). The LNA size
443 distributions are dominated by 2-4 μm particles (mean diameter: $2.99 \pm 0.06\mu\text{m}$; Supplemental Information,
444 Table S1) and dominated Atlanta PBAP composition during dry days. Many individual bacteria are likely
445 in around 1 μm , but the observed LNA particles are within the median aerodynamic diameter of culturable
446 bacteria (~ 4 μm) in continental sites (Despres et al., 2012). Bacteria in the atmosphere can be co-emitted
447 together with larger particles (e.g. soil, plant fragments) and occasionally they are observed as clumps of
448 bacteria cells (Burrows et al., 2009). In addition, several bacterial species observed in the atmosphere
449 (Delort and Amato, 2018; Monier and Lindow, 2003; Baillie and Read, 2001) are within this sizes range
450 (e.g., *Sphingomonas spp.*: 1.0 - 2.7 μm ; *Methylobacterium spp.*: 1- 8 μm , *Pseudomonas syringae*: ~2.5 μm ,
451 and *Bacillus anthracis*: 3-10 μm), supporting LNA population may represent single or agglomerated
452 bacterial cells. However, it is clear that heterogeneous populations will probably contain multiple types of
453 microorganisms and that may be the case in the LNA population.

454 It is known that pollen may burst into tiny fragments when is suspended in water (e.g., Augustin et al.,
455 2012; Taylor et al., 2007), potentially increasing the concentration of LNA particles and biasing
456 concentrations. Although 0.2 μm – 5 μm pollen fragments can be generated upon rupture, pollen (e.g. Birch,
457 Ryegrass, Oak, Olive) mainly breaks apart into submicron fragments by hydrolysis and favors
458 fragmentation into small submicron (<1 μm) particles (Taylor et al., 2007; Bacsı et al., 2006; Grote et al.,
459 2003), not considered in our FCM analysis. An additional factor to consider in pollen fragmentation is the
460 number of fragments generated per pollen grain. FCM applied to ragweed pollen suggests a 1:2 pollen-to-
461 pollen fragments concentration ratio (Supplementary information, Table S2). Also, calculations based upon
462 FCM-derived ragweed pollen and pollen fragments concentrations during this study (considering the total
463 pollen mass added to the sample, 15 μm mean diameter previously determined by Lin et al. (2013) and unit
464 density) suggest approximately 67% of the ragweed pollen grains were intact after hydration and that each
465 fragmented grain generates ~5 pollen fragments; in agreement with Bacsı et al. (2006), 35% of ragweed
466 pollen fragments upon hydration. Overall, ragweed pollen results suggest FCM experiments do not have a

467 considerable impact in pollen fragmentation and that pollen fragmentation will have a negligible effect on
468 LNA concentrations. Ragweed pollen is one of the most abundant wind-driven pollen species in the United
469 States and its emission peaks during fall, but can be also present during late spring and summer. It is
470 representative of the pollen species we see in the Atlanta area (Darrow et al., 2012) and results suggest
471 pollen fragmentation would not generate a substantial amount of fragments. The low collection efficiency
472 of SpinCon toward large particles (<14% for diameters above 5 μ m) and that pollen concentrations in our
473 samples are generally two orders of magnitude lower than LNA concentrations (Figure S22; supplemental
474 information) suggest a negligible effect of pollen fragments in LNA biological particle quantification.
475 Pollen concentrations are 100-1000 times lower than bacteria concentrations in the atmosphere (Hoose et
476 al.,2010). At least 100 supermicron (>1 μ m) pollen fragments will have to be released per pollen grain to
477 considerably influence the LNA population, which has not been observed. Also, EPM results showed intact
478 pollen and limited amounts of small debris among the particles identified in the atmospheric samples
479 collected for this study. Particles with fluorescence intensities above the FL1-A threshold value in the LNA
480 population were counted as biological, giving us the PBAP counts within the LNA population and will be
481 referred henceforth as the “LNA-AT” population (Figure 2), where “AT” refers to above threshold.

482

483 The LNA population shows SYTO-13 fluorescence intensities that are about one order of magnitude
484 lower than the HNA population, and the fluorescence intensity difference is consistent across all sampling
485 events. Based on Bouvier et al.2007, cell populations with different metabolic activity (e.g. active and non-
486 active), when detected by FCM, should observe a decrease in fluorescence intensity in consecutive
487 sampling events if transition from the HNA to the LNA population, or vice-versa if transition from LNA to
488 HNA population. The fluorescence intensity of the LNA and HNA populations show small variation
489 throughout the sampling events (LNA-AT: $7.38 \times 10^4 \pm 1.39 \times 10^4$; HNA: $6.72 \times 10^5 \pm 2.30 \times 10^5$; Table
490 S3) and no anticorrelation is observed in the studied parameters (FSC-A, SSC-A, FL1-A), which supports
491 we have in fact two distinctive population of bioaerosols (Supplemental Information; Figures S23 and S15).

492 A population of strongly fluorescing and very large particles (10-20 μ m, avg. average geometric mean
493 diameter $12.3 \pm 1.7\mu$ m) was identified (Figure 2). This population also strongly autofluoresces in the FCM
494 when SYTO-13 was not added to the sample (SI.7, Figure S11). All together this indicates a population of
495 pollen particles, as they are known to contain cell wall compounds (i.e., phenolic compounds, carotenoid
496 pigments, Phenylcoumarin) that fluoresce more strongly than the proteins and cytosolic compounds
497 responsible for bacteria/fungi autofluorescence (Pöhlker et al., 2012; Hill et al., 2009; Pöhlker et al., 2013).
498 The pollen population was not well-defined during all sampling events; whenever present, pollen was
499 characterized by concentrations ($\sim 10^2 \text{ m}^{-3}$) consistent with reported values (Despres et al., 2012), which are
500 also much lower than LNA-AT and HNA concentrations. As a result, pollen population was systematically

501 gated using a perfect square between 10^6 and 10^8 intensity units in the FL1-A vs. SSC-A plot for each
502 atmospheric sample. LNA-AT, HNA and pollen counts, acquired by the 42k threshold approach were used
503 to calculate liquid-based (mL^{-1} of sample solution) and air-based (m^{-3} of air) concentrations for each
504 bioaerosol population as detailed in the Supplemental Information. The total PBAP concentration on each
505 sample consisted of all non-bead particles above the 42k fluorescence threshold given that a non-negligible
506 biological particle concentration was not constrained in the gated populations. Even though the 2% contour
507 plots effectively allowed population gating, $16.5 \pm 7.3\%$ of the total PBAP are not attributed the identified
508 populations. The biological particles not constrained by FlowJo 2% gating, henceforth named as the
509 “unclassified” bioparticles, showed the highest concentrations when both HNA and LNA populations are
510 densely populated (4/16, 4/28 and 5/14; Figure 5). The lowest concentrations were observed when just the
511 LNA population is identified (4/9, 4/22, 5/15; Figure 5) and when the LNA and HNA populations are
512 identified after the rain event on 4/14. The observed behavior shows that the unclassified bioparticle
513 concentrations is linked to the heterogeneity of the biological populations and the concentration of the gated
514 populations (e.g. HNA, LNA and Pollen). The “unclassified” bioparticles concentration ranges from $8.1 \times$
515 10^2 m^{-3} to $1.3 \times 10^4 \text{ m}^{-3}$ (avg. $4.2 \times 10^3 \pm 3.3 \times 10^3$) and they are not constrained to a specific size range.
516 Most of the unclassified bioparticles are far from the centroids of the gated populations. They can indeed
517 be formed by fragmentation or accretion, or also be related to plant debris (i.e., irregular bioparticles) that
518 are characterized by a very broad size, internal complexity and nucleic acid content distributions. In
519 addition, we must note that additional concentration corrections are required owing to the sampling
520 efficiency of the SpinCon II, but will be considered in sections 4.3 and 4.4.

521 Before SpinCon II sampling efficiency corrections are applied, FCM total particle concentrations range
522 from $2.6 \times 10^4 \text{ m}^{-3}$ to $2.9 \times 10^5 \text{ m}^{-3}$, with increasing concentrations toward the end of the sampling period.
523 In addition, total PBAP concentration averaged $2.4 \times 10^4 \pm 1.1 \times 10^4 \text{ m}^{-3}$ (coefficient of variation, CV, 13%;
524 defined as the standard deviation over a triplicate FCM measurements over the average concentration).
525 LNA-AT ranged between 6.8×10^2 and $2.9 \times 10^4 \text{ m}^{-3}$ (average: $1.1 \times 10^4 \text{ m}^{-3}$; CV: 20%), HNA (fungal spores)
526 between 4.7×10^3 and $1.9 \times 10^4 \text{ m}^{-3}$ (average: $1.1 \times 10^4 \text{ m}^{-3}$; CV: 15%) when above the detection limit (n=12),
527 and pollen from 1.3×10^2 to $1.2 \times 10^3 \text{ m}^{-3}$ (average: $3.6 \times 10^2 \text{ m}^{-3}$; CV: 21%). These concentration levels are
528 consistent with microscopy-based studies in urban environments for bacteria (e.g., $1.7 \times 10^4 \pm 1.3 \times 10^4 \text{ m}^{-3}$
529 in springtime Birmingham, UK; (Harrison et al., 2005); fungal spores ($1.8 \times 10^4 \pm 1.1 \times 10^4 \text{ m}^{-3}$ in Vienna,
530 Austria between April-June; Bauer et al., 2008); and pollen (between $5.69 \times 10^2 \text{ m}^{-3}$ to $6.144 \times 10^3 \text{ m}^{-3}$ in
531 Medellin, Colombia; Guarín et al., 2015). Also, additional experiments performed in September 2015,
532 described in Figure S7 of the supplemental information (supplemental information, SI.6), showed that EPM
533 and FCM-based quantifications agree within an order of magnitude. This is consistent with Lange et al.

534 (1997), whom also found that FCM gives higher quantifications than EPM microscopy when studying *P.*
535 *aeruginosa* pure cultures and airborne bacteria collected from a swine confinement building in Iowa, USA.

536 To better understand SYTO-13 fluorescence intensity differences between the identified (e.g. LNA-
537 AT, HNA and pollen) populations in the atmospheric samples and their metabolic/stress state, FCM
538 experiments were conducted with air-isolated bacteria (F8 strain; De Leon Rodriguez, 2015), ragweed
539 pollen and yeast (*S. cerevisiae*; Y55 strain) mixtures to compare the SYTO-13 fluorescence intensity and
540 the scattering properties of the pure cultures to those seen in the atmospheric samples. Pure culture
541 experiments aimed to: (1) serve as positive controls to ensure SYTO-13 effectively stains bacteria, fungi
542 and pollen, and (2) acquire reference fluorescence and scattering properties on each pure culture population.
543 Pure cultures and atmospheric samples are summarized in Tables S3, S4 (supplementary information; FCM
544 pure culture experiments) respectively. The LNA-AT population showed SYTO-13 fluorescence intensity
545 up two orders of magnitude lower than F8 bacteria. The HNA population showed an order of magnitude
546 lower SYTO-13 fluorescence intensity than Y55 HNA yeast, and, within the same magnitude for the LNA
547 Y55 yeast. The HNA and LNA yeast populations in the pure culture experiments (Figure S13a) have one
548 order of magnitude difference in FL1-A fluorescence intensity and may represent yeast populations with
549 different metabolic states. Atmospheric and ragweed pollen populations had similar SYTO-13 fluorescence
550 intensities and Figure S13c shows pollen fluorescence intensity may go up to 10^8 . The lower SYTO-13
551 fluorescence intensity of the atmospheric populations may be related to genetic material degradation from
552 exposure to atmospheric stressors; depending on the physiological characteristics of each population (Zhen
553 et al., 2013; Amato et al., 2015). Our results also agree with Guindulian et al. (1997), showing that *E.coli*
554 overnight cultures have higher SYTO-13 fluorescence intensity than starved *E.coli* population. Overall,
555 FCM pure culture results suggest microbes starve in the atmosphere, leading to a possible reduction or
556 leakage of the amount genetic material enclosed within each cell. Sampling can also stress cells, even
557 disrupt the wall/membrane of the cell and lead to genetic material leakage (Zhen et al., 2013).

558 Pollen, HNA and LNA-AT atmospheric populations showed different SYTO-13 fluorescence
559 intensities. Pollen showed the highest fluorescence intensity, followed by the HNA and LNA-AT (fraction
560 of LNA above threshold; Figure 2) populations, respectively (Figure 2; Table S4). Guindulian et al. (1997)
561 FCM results with starved bacterioplankton from seawater samples treated with DNase/RNase showed
562 SYTO-13 fluorescence intensity can be related to the DNA content of starved bacterioplankton due to the
563 low amount of RNA enclosed in starved cells. Taking in consideration our results and previous studies, we
564 can suggest that Pollen, LNA-AT and HNA populations in the atmospheric samples are differenced by their
565 DNA content, which can in part explain SYTO-13 fluorescence intensity difference between them. We also
566 acknowledge DNA sequestration by bacteria, fungal spores and pollen may differ and their cell membrane

567 characteristics will ultimately determine how much stress the cells will sustain before they completely
568 rupture. SYTO-13 is a highly permeable stain and effectively detects nucleic acids (DNA and RNA) of
569 bacteria endospores and vegetative cells (Comas Riu et al.,2002). Fungal spores have also been effectively
570 stained by DNA/RNA probes (Bochdansky et al., 2017; Chen and Li et al., 2005), but some fungal spores
571 might not be equally stained due to their harder cell wall, and chromatin-binding of DNA (Standaert-Vitse
572 et al., 2015). Future work is needs to further study this.

573 **4.2 WIBS total concentration and FBAP daily variability**

574 WIBS-4A collected data continuously throughout the period; for comparison against the SpinCon
575 II 4h liquid batch samples, WIBS data was averaged to the SpinCon II sampling times (Table 1). WIBS
576 total particle concentration (1-5 μ m diameter) ranged from 2.0×10^5 to 1.0×10^6 m⁻³ in agreement with
577 observed particle concentrations in previously studied urban environments during Spring/Summer months
578 like Helsinki, Finland (UV-APS avg. 1.6×10^5 m⁻³; Saari et al., 2014) and Karlsruhe, Germany (WIBS-4
579 avg. 6.9×10^5 m⁻³; Tropak and Schnaiter et al., 2013). 4h average total particles concentrations in Figure 3a
580 show particle concentrations declined during rain episodes (during or post-rain: e.g. 4/15, 4/16, 4/28, 4/29,
581 4/30) as wet removal of PBAP is most efficient. However, during dry (no rain) episodes total particle
582 concentrations built up in the atmosphere. To better understand the day-to-day variability of different FBAP
583 types, the seven Perring et al. (2015) FBAP categories (e.g. Type A, B, C, AB, AC, BC and ABC) were
584 studied plus the NON-FBAP type constituting particles that do not fluoresce in any channel (e.g. channel
585 A, B, C). NON-FBAP concentrations are one order of magnitude higher than FBAP concentrations, and
586 NON-FBAP, hence traced WIBS total particles throughout all sampling events (Figure 3a). Total FBAP
587 concentrations also show similar behavior to the total particle concentration (Figure 3a) and it suggests non-
588 biological particles can be biasing the total FBAP concentration. The variability of the total FBAP
589 concentration is mainly linked to type A and type B concentrations as overall they constitute the two largest
590 fractions to the total FBAP concentration (Figure 3b), and both FBAP types have previously misidentified
591 non-biological particles as FBAP (Tropak and Schnaiter et al., 2013; Yu et al., 2016). As a result, our study
592 considers the total FBAP concentration as the upper limit, and ABC type concentration as the lower limit
593 of FBAP concentration in Metro, Atlanta. Type B dominates the FBAP fractional composition (Figure 3b),
594 which has been linked to possible non-biological interferences from black carbon (Yu et al., 2016) and
595 polycyclic aromatic hydrocarbons (PAHs) emitted from combustion sources. Total FBAP fraction ranges
596 from 16% and 43%, and ABC fraction ranges from 1.3% and 9.2% of the total particles in the 1 to 5 μ m
597 size range. ABC type fractions and ABC type concentrations are within the values observed by Tropak and
598 Schnaiter (2013) using WIBS-4 in Karlsruhe, Germany; averaging 2.9×10^4 m⁻³ (when considering the sum
599 of AC and ABC types) and constituting 7% of total coarse mode particles (0.8 μ m-16 μ m).

600 ABC type concentrations show an interesting variability throughout the 15 sampling events, as
601 ABC reaches its maximum concentration on 4/14, on a warm and humid day after a rain event, concurrently
602 when the FCM HNA population also reaches its highest concentration – strongly suggesting ABC particles
603 are fungal spores. (Figure 3a, Table 1). Furthermore, WIBS high resolution data in Figure S24 shows the
604 enhancement of AB and ABC type right after the beginning of the rain event on 4/13 (6pm; night before
605 sampling on 4/14) and is not correlated to NON-FBAP concentrations; FBAP concentration enhancement
606 previously linked to wet-ejected fungal spores (Huffman et al., 2013; Gosselin et al., 2016). Gosselin et al.
607 (2016) used WIBS-3 in the Rocky Mountains, Colorado showing ABC type fractional composition
608 enhances after rain events to dominate the total FBAP composition and the enhancement is correlated to
609 mannitol and arabitol concentrations (fungal spore tracers), which have been previously linked to
610 Ascomycota and Basidiomycota spores emitted by the wet-ejection mechanism (Elbert et al., 2007). In
611 addition, ABC type constitute a considerable fraction ($\sim 20\%$) of total FBAP during dry days in the Rocky
612 Mountains possible because such highly vegetative environments maintain a high background of fungal
613 spores (Huffman et al., 2013). However, urban environments like Metro Atlanta are not necessary
614 dominated by fungal spores and its FBAP composition will be affected by the biological sources close to
615 city (e.g. forests), local emissions and meteorology. The overall FBAP composition in metro Atlanta
616 (Figure 3b) is dominated by type B (avg. fraction: $33 \pm 9\%$), type A (avg. fraction: $22 \pm 5\%$) and type AB
617 (avg. fraction: $22 \pm 5\%$) particles. Type ABC constitute $12 \pm 6\%$ of the total FBAP and it reaches 30% on
618 4/14, comparable to values observed by Gosselin et al., 2016 in the Rocky Mountains. The dominance of
619 type B particles has been observed in the polluted atmosphere of Nanjing, China using WIBS-4A were type
620 B constituted $\sim 45\%$ of the total PBAP and type B ($\sim 2 \times 10^6 \text{ m}^{-3}$) concentrations were up to two orders of
621 magnitude higher than type A concentrations ($\sim 5 \times 10^4 \text{ m}^{-3}$) suggesting a high likelihood of interference
622 from abiotic particle sources. However, Metro-Atlanta shows much lower total particle concentrations than
623 Nanjing, China ($\sim 10^7 \text{ m}^{-3}$) and type A and type B concentrations are within the same order of magnitude.
624 Furthermore, Perring et al. (2015) have shown type B particles constitute a considerable fraction of the total
625 supermicron particles across the United States, being $\sim 15\%$ and $\sim 25\%$ over (altitude $>100\text{m}$) the
626 Southeastern US and Southwestern US, respectively. Total particle and NON-FBAP size distributions in
627 Figure 3c peaked at $\sim 1\mu\text{m}$. Similarly, types A, B, AB size distributions (Figure 3d) peaked close to $1\mu\text{m}$
628 showing that interferences by non-biological particles cannot be rule out. However, ABC type size
629 distribution (light blue line, Figure 3d) is dominated by $3\text{-}5\mu\text{m}$ particles and ABC type particles may have
630 come from a different source to other FBAP types as they get enhanced after rain events (e.g. 4/14; Table
631 1). Yu et al. (2016) also observed $4\text{-}6\mu\text{m}$ ABC type particles in the highly polluted Nanjing, China, but
632 ABC type bimodal size distributions showed a peak between $1\text{-}2\mu\text{m}$ and a second peak between $4\text{-}6\mu\text{m}$. In
633 addition, ABC type number fractions in Nanjing, China correlated to black carbon mass fractions

634 suggesting a considerable influence by combustion related particles and no rain events occurred during the
635 sampling period. The difference between Metro Atlanta and Nanjing, China ABC type size distributions
636 suggest ABC type is not influenced by combustion related particles in Metro Atlanta. Overall, results show
637 FBAP concentration (1-5 μm) ranges from 10^4 - 10^5 m^{-3} in metro Atlanta and wet-ejected fungal spores
638 concentration, detected by ABC type, can constitute up to 30% of the FBAP (1-5 μm) after rain events.

639 **4.3 Correlation of HNA population with ABC type**

640 A quantitative comparison between WIBS-4A total particle and FCM total particle concentrations
641 was subsequently performed and we focused the analysis to the 1 to 5 μm size range as SpinCon sampling
642 efficiency is reduced significantly above 5 μm ($\leq 14\%$; Kesavan et al., 2015). WIBS-4A and FCM total
643 particle concentrations differed by about one order of magnitude (for optical diameter, d_o , greater than
644 1.5 μm) and particle concentration difference increased for particles with $d_o < 1.5 \mu\text{m}$ as shown in the size
645 distribution (geometrically averaged across the 15 SpinCon II sampling events) in Figure 4a. The largest
646 difference between WIBS-4A and uncorrected FCM size distributions seems to be related to SpinCon II
647 having a cutoff size close to 1 μm , reducing significantly its sampling efficiency. Even with the observed
648 difference in the magnitude of the concentrations between the two techniques, ABC type and HNA
649 concentrations traced throughout all the sampling events and are moderately correlated ($R^2 = 0.40$, P-value
650 = 0.016; Figure 4b) and showed similar size distributions in the 1 to 5 μm range as shown in Figure S12a.
651 HNA and ABC type were both dominated by 3-5 μm particles and it seems both are detecting the same
652 type of biological particles. In addition, AB type showed a weak correlation with HNA concentrations (R^2
653 = 0.17), but their size distributions differed as type AB peaks close to $\sim 1\mu\text{m}$ (Figure 3d). ABC is the only
654 FBAP type showing a considerable correlation to the HNA population, and LNA-AT population is not
655 correlated with any FBAP type. Overall, ABC type and HNA correlation is an important step forward to
656 better understand the effectiveness of WIBS-4A FBAP categories to provide speciated PBAP
657 concentrations in urban areas. ABC type particles have shown substantial concentrations (10^4 - 10^5 m^{-3} ;
658 Perring et al., 2015; Ziemba et al., 2016) across the US. The highest ABC fraction of the total FBAP was
659 observed in Panhandle, Florida during an airborne study among multiple environments studied using
660 WIBS-4A to sample from the California coast to central Florida, suggesting ABC type particles are
661 ubiquitous in the US (Perring et al., 2015). Previous studies (Healy et al., 2014, Huffman et al., 2013) have
662 shown correlations between LIF technology (e.g. WIBS-4 and UV-APS) fluorescence channels and fungal
663 spores number concentrations, especially during fungal spores invigoration after rain events. Healy et al.
664 (2014) used WIBS-4 in Killarney National Park, Ireland (e.g. high vegetative rural area) finding correlations
665 between channel B (FL2; $R^2 = 0.29$) and channel C (FL3; $R^2 = 0.38$) concentrations and fungal spores
666 concentrations (collected by Sporewatch impactor and quantified by microscopy). Gosselin et al. (2016)
667 observed stronger correlations between fungal spores (inferred from mannitol and arabitol concentrations)

668 and WIBS-4 concentrations in the Rocky Mountains, but our study in Atlanta, GA was carried out in
669 completely different environment (e.g. highly-populated urban environment). Now for the first time FCM
670 HNA population have shown a correlation with WIBS-4A ABC type and suggests ABC type category
671 detects wet actively ejected fungal spores in Metro Atlanta (e.g. urban area). In addition, recent WIBS-4A
672 experiments using pure cultures have shown ABC type detects well several fungal spores (e.g. *Aspergillus*
673 *Versicolor* & *Botrytis spp.*) and small pollen grains, but detection may vary across instruments (Hernandez
674 et al., 2016).

675 FCM concentrations were corrected based on correction factors (CF) calculated upon the
676 comparison of ABC and HNA size distributions (1 to 5 μ m) for each sampling event given (1) ABC type
677 and HNA population similar size distributions and number concentrations (1 to 5 μ m) correlation, and, (2)
678 WIBS-4A provides us representative concentrations of airborne particle concentrations in Metro Atlanta
679 after sampling losses being corrected (Section 3.2). Concentration correction factors were determined for
680 each sampling episode by taking the quotient of ABC type to HNA concentrations over the 1-5 μ m size
681 range. The resulting size-dependent correction factor (Figure S12b) was then applied to the FCM size
682 distributions, giving the “corrected FCM” bioaerosol data (between 1 and 5 μ m). Figure 4a shows that the
683 corrected FCM total particle average size distribution traces WIBS-4A size distribution, allowing us to
684 correct for SpinCon II low collection efficiency and to better constrain the magnitude of FCM
685 concentrations. Our approach to calculate the estimated collection efficiency (ECE) considers all the
686 processes that affect the concentration of PBAP, from collection to final quantification in the FCM. Figure
687 S12b compares Kesavan et al. (2015) collection efficiencies determined for SpinCon I and the estimated
688 collection efficiency calculated upon the CF calculation ($ECE = 1/CF$) and shows the ECE of the SpinCon
689 II is lower than Kesavan et al. (2015) below 3 μ m and performs better for particles above 3 μ m, but above
690 3 μ m Kesavan et al (2015) collection efficiency is within the uncertainty of our calculations. Our lower ECE
691 values (Figure S12b) for particles below 3 μ m can be related to SpinCon sampling time as Kesavan et al.
692 (2015) experiment were conducted in a short period of time (e.g. 10-15 min) and ours took place for 4 h
693 The main mechanisms leading to below 3 μ m particle losses could be their re-aerosolization over time being
694 lost through the blower exhaust of the SpinCon II (Figure 1). Also, coagulation of small particles over time
695 can not be rule out, but future work is needs to study it. Although SpinCon/FCM results correction based
696 on the HNA and ABC type size distributions comparison effectively constrain the efficiency of the
697 SpinCon/FCM analysis in this study, corrections are limited to the 1 to 5 μ m size range and must
698 acknowledge that the specific sampling may stress cells and affect their detection.

699

700 **4.4 PBAP populations after collection/detection corrections**

701 After correction through the application of the ABC correction factors, FCM total particle
702 concentrations (1 to 5 μ m avg.: $5.5 \times 10^5 \pm 5.1 \times 10^5$ m⁻³; Figure 5a) are within the same order of magnitude
703 as WIBS-4A concentrations (1 to 5 μ m avg.: $5.4 \times 10^5 \pm 2.9 \times 10^5$ m⁻³; Figure 3a), and continue to exhibit
704 substantial variability. The HNA (e.g. fungal spores) population showed a substantial invigoration during
705 three sampling events (4/7, 4/14, 4/15; Figure 5a and 5b). To better understand the role of meteorology on
706 PBAP composition, 24 hr-averaged temperature and relative humidity were used to express the prevailing
707 temperature and relative humidity (RH) during each sampling event, considering the residence time of
708 microorganisms (e.g. bacteria and fungal spores) before sampling. Sampling events were classified into
709 four regimes based on the average diurnal (24hr avg.) relative humidity and ambient temperature, with T=
710 18 °C (65 °F) to differentiate between warm and cold days, and, RH = 70% to differentiate between humid
711 and dry days. During the 15 sampling days, temperature ranged from 10.4°C to 31.2°C, and RH varied from
712 19.0% to 97.0% in Atlanta, GA (Look Table S4; supplemental information) The temperature and RH
713 threshold values were chosen based on the observations and understanding that a combination of
714 temperature and RH within these threshold values can significantly impact bioaerosol composition. For
715 instance, humid and warm conditions may lead to the invigoration of fungal spores by wet ejection from
716 plants (Ingold, 1971), on contrary, PBAP will get stressed when exposed to warm and dry conditions. The
717 sampling times, RH, ambient temperature and meteorological categories of each SpinCon II sample is
718 presented in Table 1.

719 Humid and warm days (4/7, 4/14 and 4/15; light green shaded areas in Figure 5a) were characterized
720 by well-defined HNA and LNA-AT populations. These sampling episodes had the highest average HNA
721 (fungal spore) concentration ($4.0 \times 10^4 \pm 1.3 \times 10^4$ m⁻³) among the four meteorological regimes and during
722 these sampling events HNA constituted ≥ 77 % of the total PBAP. Among the humid and warm days (Figure
723 5a and 5b), average LNA-AT, HNA and “unclassified” bioaerosol compositions were 6.1%, 84.0% and
724 9.9%, respectively of the total PBAP number. Also, the humid and warm days occurred after rain events,
725 which can be linked directly to the strong fungal spore invigoration (Huffman et al., 2013). Before sampling,
726 early morning precipitation occurred during 4/14 and 4/15, as well as during the night of 4/6. Precipitation
727 did not occur during sampling in any of the humid and warm days. The FCM results (Figure S15a-c) that
728 display the PBAP population between 4/7 and 4/9 show a disappearance of the (HNA) fungal spore
729 population during the transition from a “humid and warm” day (4/7) to a “dry and warm” day (4/9). Figure
730 5b shows how the HNA contribution to the total PBAP goes down on 4/8 when RH decreases and is
731 undetected on 4/9. Furthermore, Figure 6a-c shows FL1 vs. SSC-A plots for 4/14 to 4/16 consecutive
732 sampling periods, where a marked increase in the LNA-AT concentration from 4/15 to 4/16 goes together
733 with a striking decrease in the HNA concentration. HNA fraction went down from 92.0% to 34.1% of the

734 total PBAP and LNA-AT concentration went up from $3.8 \times 10^3 \text{ m}^{-3}$ to $2.9 \times 10^4 \text{ m}^{-3}$. Humid and Warm days
735 had the lowest averaged PBAP concentration ($4.6 \times 10^4 \pm 9.8 \times 10^3 \text{ m}^{-3}$ in the 1 to $5 \mu\text{m}$ range) among the
736 four meteorological regimes, a possible effect of the bioaerosols being lost by wet scavenging, resulting in
737 the enhancement of fungal spore contribution to the total PBAP number concentrations. The unclassified
738 biological particles concentration also showed its lowest contribution ($2.9 \times 10^3 \text{ m}^{-3}$; 9.9%) to the total
739 PBAP number concentration during these events, when the HNA and LNA populations are best identified
740 by the 2% contour plots.

741 Cold and humid days (4/16 and 4/29; light yellow shaded areas in Figure 5a) also showed well-defined
742 HNA population, and HNA contributed on average to $29.5 \pm 6.5 \%$ of the total PBAP concentration (1 to
743 $5 \mu\text{m}$). On 4/16 drizzling took place by the end of the sampling period, but no accumulated rainfall was
744 measured by the meteorological station. However, on 4/29, accumulated rainfall averaged 0.04in. from
745 11:55 AM to 2:20 PM (Figure S21). The similar HNA concentration between “Humid and Warm” and
746 “Humid and Cold” days seen in Figure 5a and the lower contribution of HNA to the total PBAP during the
747 “Humid and Cold” days may be linked to previously suggested bacteria emissions by droplet soil impaction
748 during rain events (Joung et al., 2017). Bacteria emission by soil impaction can increase airborne LNA-
749 AT concentration and HNA (fungal spores) will have a lower contribution to the total PBAP even when the
750 fungal spore concentration is high during rain events. Both cold and humid days showed a considerable
751 difference in LNA-AT contributions to the total PBAP concentration. On 4/16 and 4/29 LNA-AT
752 constituted 45.2% and 65.3% of the total PBAP concentration, respectively (Figure 5b). The difference in
753 the LNA-AT contribution to the total PBAP can be linked to the intensity of precipitation, as it shapes the
754 composition (e.g. size and types) of microbes suspended in the atmosphere during the different stages of a
755 rainfall (e.g. before, on set, during and after a rainfall; Yue et al., 2016).

756 Six of the fifteen sampling days were classified as warm and dry (4/8, 4/9, 4/22, 5/13, 5/14, 5/15; light
757 orange shaded areas in Figure 5a) and it did not rain before or during any of these days (Table 1). During
758 warm and dry days, HNA had the lowest averaged concentration ($8.7 \times 10^3 \pm 1.2 \times 10^4 \text{ m}^{-3}$) among the four
759 meteorological categories. In addition, during three dry and warm days (4/9, 4/22 and 5/15) the HNA
760 population was undetected. This behavior can be related to the fact that high RH drives fungal spore
761 emissions by wet ejection, but soil wetness could also affect emissions because the HNA population was
762 detected in other warm and dry days with comparable RH (Huffman et al., 2013; Gosselin et al., 2016). The
763 air mass trajectories reaching Atlanta during each sampling event could also affect the biological particles
764 composition. For example, on 4/22, when the HNA was undetected, the 500m and 100m 72 h backward air
765 mass trajectories reaching Atlanta came from the NW (US/Canada border) at high altitudes and do not
766 spend more than 24h near surface. This air mass could affect bioaerosol composition with minimal

767 influence from local bioaerosol emissions. However, the enhancement or the depletion of the HNA
768 population have not been linked to specific air masses trajectories. Overall, warm and dry days prevail
769 during springtime in Atlanta and LNA-AT contribution (avg.: $3.4 \times 10^4 \pm 2.5 \times 10^4 \text{ m}^{-3}$) may represent the
770 bioaerosol background of Atlanta.

771 Four of the fifteen sampling days (4/21, 4/23, 4/28 and 4/30; light blue shaded areas in Figure 5a) were
772 characterized by cold and dry conditions (Table 1). PBAP were dominated by LNA-AT during these events,
773 as can see in Figure 7a-c, where LNA population are the dominant contributors to PBAP number. HNA
774 population was diminished in Figure 7a (4/21) & Figure 7c (4/23) during cold and dry days and disappeared
775 in Figure 7b during a warm and dry day. Overall, HNA was detected during cold and dry days, but showed
776 lower contributions to the total PBAP number concentration than humid days. Among cold and dry days,
777 the PBAP population (1 to 5 μm) was composed on average of $72.6 \pm 10.1\%$ LNA-AT and $16.5 \pm 8.2\%$
778 HNA. Cold and dry days had on average the highest LNA-AT ($5.3 \times 10^4 \pm 1.8 \times 10^4 \text{ m}^{-3}$) and total PBAP
779 ($7.3 \times 10^4 \pm 2.0 \times 10^4 \text{ m}^{-3}$) number concentrations (1 to 5 μm) among the four meteorological categories,
780 reaching the PBAP maximum concentration on 4/23 (Figure 5a).

781

782 **4.5 PBAP day-to-day variability in Metro Atlanta: FCM vs. WIBS**

783 Although WIBS and FCM possess different methodologies, they show similar trends providing a
784 good understanding of the daily variability of PBAP in Metro Atlanta. FCM PBAP fraction (1 to 5 μm)
785 ranges from 3.8% to 69.2% of the total particles and the highest PBAP fraction (69.2%) and HNA
786 concentration is observed on 4/14 ($5.25 \times 10^4 \pm 5.89 \times 10^3 \text{ m}^{-3}$). The total FBAP fraction (1 to 5 μm) ranges
787 from 16% to 43%, but it reaches its maximum on 4/15. However, ABC fraction of the total WIBS particle
788 concentration ranges from 1.3% to 9.2% and it reaches its maximum on 4/14. Even when the magnitudes
789 of the PBAP and FBAP fractions differ on average by a factor of ~ 2 throughout the sampling period, both
790 techniques agree an enhancement in the total biological particles takes place between 4/14 to 4/16. Given
791 the uncertainty of the two methodologies, it is remarkable that there is such agreement between WIBS and
792 FCM results.

793 Among the four meteorological categories, humid and warm days characterize for showing the
794 highest HNA, A type, AB type and ABC type concentrations suggesting that A and AB types may also be
795 related to wet-ejected fungal spores in Metro Atlanta; this possibly explains why the ABC fraction of the
796 total FBAP in 4/7 is not as high as on 4/14 and 4/15 (Figure 3b), and differs with the behavior observed by
797 the HNA population on 4/7. The LNA-AT population does not show a correlation to any specific FBAP
798 type and shows its highest concentrations during dry and cold days. In addition, LNA-AT concentrations are
799 anticorrelated with type B concentrations (Figure S19, correlation coefficient, $r = -0.59$; $R^2 = 0.30$) during

800 dry (both cold and warm) days, when LNA-AT dominates the total PBAP concentration. Given that type B
801 particles have been previously correlated to abiotic particles (e.g. black carbon) in urban environments (Yue
802 et al., 2017), LNA-AT and type B anticorrelation suggests that LNA-AT particles may in fact represent a
803 heterogeneous bioaerosol population. That LNA-AT is not correlated with any FBAP type gives rise to two
804 possibilities: (1) if LNA-AT population is mainly composed of bacteria or agglomerated bacteria, then it is
805 possible that they are detected by multiple FBAP types and is not attributed specifically to one of them; (2)
806 the intrinsic fluorescence of LNA-AT particles is too low and a high fraction of them is abiotic. It is
807 challenging to determine what PBAP types each WIBS FBAP type is mainly detecting. Based on WIBS-
808 4A results in Metro Atlanta, ABC type detects wet-ejected fungal spores, but still unclear what PBAP types
809 are detected by the other FBAP types or if they just capture a high fraction of non-biological particles. FBAP
810 types and WIBS total particles correlations in Figure S17 show all FBAP types are correlated to WIBS total
811 particles, but ABC and AB types show the lowest correlations (type AB: $R^2 = 0.101$; type ABC: $R^2 =$
812 0.1266).

813 Figure 8 shows FCM total PBAP (black line), ABC type (light green), FL1(Channel A; dark green
814 line) and total FBAP (blue line) concentrations, where the FL1 concentration ([FL1]) constitutes the sum
815 of the number concentrations of types A, AB, AC, and ABC ([FL1] = [A] + [AB] + [AC] + [ABC]; Gabey
816 et al., 2011; Healy et al., 2014). Throughout the April-May 2015 sampling events, total PBAP
817 concentrations (1 to 5 μ m) were mainly constrained between the FL1 and ABC type concentrations
818 suggesting FL1 and ABC type represent the upper and lower bound PBAP concentrations in Metro Atlanta,
819 respectively. It is also important to highlight that FCM PBAP concentrations are closer to the ABC type
820 concentrations before April 16 when the HNA population dominates, but then after April 16 FCM PBAP
821 concentrations are closer to FL1 concentrations when LNA-AT starts to dominate the total PBAP
822 concentration. In addition, Figure 8 shows that total FBAP (sum of type A, B, C, AB, AC, ABC) exceeds
823 the (corrected) PBAP concentrations in Metro Atlanta.

824 **5. Conclusions**

825 In this study we presented the development and testing of an effective FCM protocol to identify and
826 quantify bioaerosol populations. The FCM protocol, designed to constrain any particle accumulation due
827 to cleaning or by fluid supplies, successfully quantified the day-to-day variability of bioaerosols in the
828 Atlanta Metro area. It is the first FCM study to detect well-defined LNA (low nucleic acid) and HNA (high
829 nucleic acid) atmospheric biological populations under different meteorological scenarios. FCM results
830 show dynamic bioaerosol populations in Atlanta leading to a 84.0% of HNA (wet-ejected fungal spores)
831 and 6.1% LNA-AT contribution to the PBAP number (1 to 5 μ m range), respectively, during humid and

832 warm days after rain events. However, LNA-AT dominates warm and cold dry days, constituting 72% of
833 the PBAP number concentration.

834 WIBS-4A and SpinCon II collocated sampling showed that the HNA and ABC type concentrations are
835 well correlated ($R^2=0.40$) and display similar size distributions. We therefore conclude that both
836 instruments detect the same particles, and used empirical collection/detection efficiency factors to correct
837 the FCM size distributions and concentrations in the 1 to 5 μm diameter range. WIBS-4A and FCM results
838 suggest Metro Atlanta PBAP concentrations range between $10^4 - 10^5 \text{ m}^{-3}$ (1 to 5 μm) and they can constitute
839 a substantial fraction of coarse mode particle concentration (WIBS-4A: 43%; FCM: 69%), comparable to
840 the PBAP coarse mode fraction in highly vegetated environments. The FCM LNA-AT population, possibly
841 containing bacterial cells, did not correlate to any FBAP type. The fact that the LNA-AT population is not
842 correlated with a specific FBAP type suggests it may be particularly challenging to use LIF techniques to
843 distinguish bioaerosols with low intrinsic autofluorescence from non-biological particles, especially given
844 the heterogeneities introduced by the large biodiversity of airborne microbes. The possible influence of
845 abiotic particles in the LNA-AT population can also explain the lack of correlation between LNA-AT and
846 FBAP types given that the FCM threshold approach does not ensure total exclusion of abiotic particles. In
847 addition, the unspecific binding of SYTO-13 to abiotic particles cannot be ruled out in the LNA-AT
848 population. FCM comparison between atmospheric and pure culture samples showed lower SYTO-13
849 fluorescence intensities in the atmospheric samples and suggests a degradation in the genetic material of
850 PBAP, possibly caused by the limited nutrients and strong stress prevailing in the atmosphere, which further
851 challenge the ability of LIF to distinguish LNA-AT.

852 In summary, this study has shown for the first time that FCM can effectively identify, quantify and
853 study the daily variability of heterogeneous PBAP populations (e.g. HNA, LNA-AT and pollen) with
854 different genetic material content in atmospheric samples. We also show that a number of FCM and WIBS-
855 4A populations are largely correlated and therefore can be used to identify the nature of the FBAP detected
856 in the latter. Our results finally show that the detection and quantification of bacterial cells in atmospheric
857 samples remains a challenging task and is best achieved through the combination of techniques.

858

859 **Acknowledgments**

860 We acknowledge support from a Georgia Power Faculty Scholar chair, a Cullen-Peck Faculty Fellowship,
861 a Dreyfus Foundation Postdoctoral Fellowship in Environmental Chemistry, NASA, a NASA Earth System
862 Science Fellowship (grant no. 80NSSC17K0434). We also acknowledge support from project PyroTRACH
863 (ERC-2016-COG) funded from H2020-EU.1.1. - Excellent Science - European Research Council (ERC),

864 project ID 726165. We also thank Prof. Rodney Weber for helpful suggestions on the SpinCon II flow
865 calibration.

866

867 **Competing interests**

868 The authors declare no competing interests.

869

870 **Author contributions**

871 AN, AN, KK and MB conceived the study. AN, NDLR, SW developed the modified biosampler. AN and
872 NDLR developed the FCM analysis and sampling protocol. AN, NDLR carried out measurements, and SW
873 helped support with analysis of the biological samples. LZ, BA provided the WIBS and helped with its
874 setup and initial data analysis procedure. AN, AN worked on the analysis, write codes to interpret the data
875 and developed the analysis protocol to combine the FCM and WIBS analysis outlined here. AN and AN
876 wrote the paper, and all authors contributed with comments and modified text.

877

878 **References**

- 879 Amato, P., Joly, M., Schaupp, C., Attard, E., Möhler, O., Morris, C. E., Brunet, Y., and Delort, A. M.:
880 Survival and ice nucleation activity of bacteria as aerosols in a cloud simulation chamber, *Atmospheric*
881 *Chemistry and Physics Discussions*, 15, 4055-4082, 10.5194/acpd-15-4055-2015, 2015.
- 882 Augustin, S., Hartmann, S., Pummer, B., Grothe, H., Niedermeier, D., Clauss, T., Voigtländer, J.,
883 Tomsche, L., Wex, H., and Stratmann, F.: Immersion freezing of birch pollen washing water,
884 *Atmospheric Chemistry and Physics Discussions*, 12, 32911-32943, 10.5194/acpd-12-32911-2012, 2012.
- 885 Bacsi, A., Choudhury, B. K., Dharajiya, N., Sur, S., and Boldogh, I.: Subpollen particles: carriers of
886 allergenic proteins and oxidases, *J Allergy Clin Immunol*, 118, 844-850, 10.1016/j.jaci.2006.07.006,
887 2006.
- 888 Baillie, L., and Read, T. D.: *Bacillus anthracis*, a bug with attitude!, *Current Opinion in Microbiology*, 4,
889 78-81, [https://doi.org/10.1016/S1369-5274\(00\)00168-5](https://doi.org/10.1016/S1369-5274(00)00168-5), 2001.
- 890 Bauer, H., Claeys, M., Vermeylen, R., Schueller, E., Weinke, G., Berger, A., and Puxbaum, H.: Arabitol
891 and mannitol as tracers for the quantification of airborne fungal spores, *Atmospheric Environment*, 42,
892 588-593, 10.1016/j.atmosenv.2007.10.013, 2008.
- 893 Bauer, H., Schueller, E., Weinke, G., Berger, A., Hitznerberger, R., Marr, I. L., and Puxbaum, H.:
894 Significant contributions of fungal spores to the organic carbon and to the aerosol mass balance of the
895 urban atmospheric aerosol, *Atmospheric Environment*, 42, 5542-5549, 10.1016/j.atmosenv.2008.03.019,
896 2008.
- 897 Bochdansky, A. B., Clouse, M. A., and Herndl, G. J.: Eukaryotic microbes, principally fungi and
898 labyrinthulomycetes, dominate biomass on bathypelagic marine snow, *The Isme Journal*, 11, 362,
899 10.1038/ismej.2016.113, 2016.
- 900 Bouvier, T., Del Giorgio, P. A., and Gasol, J. M.: A comparative study of the cytometric characteristics of
901 high and low nucleic-acid bacterioplankton cells from different aquatic ecosystems, *Environ Microbiol*, 9,
902 2050-2066, 10.1111/j.1462-2920.2007.01321.x, 2007.
- 903 Burrows, S. M., Elbert, W., Lawrence, M. G., and Pöschl, U.: Bacteria in the global atmosphere – Part 1:
904 Review and synthesis of literature data for different ecosystems, *Atmos. Chem. Phys.*, 9, 9263-9280,
905 <https://doi.org/10.5194/acp-9-9263-2009>, 2009.
- 906 Chen, P. S., and Li, C. S.: Bioaerosol characterization by flow cytometry with fluorochrome, *J Environ*
907 *Monit*, 7, 950-959, 10.1039/b505224f, 2005.
- 908 Chi, M.-C., and Li, C.-S.: Fluorochrome in Monitoring Atmospheric Bioaerosols and Correlations with
909 Meteorological Factors and Air Pollutants, *Aerosol Science and Technology*, 41, 672-678,
910 10.1080/02786820701383181, 2007.
- 911 Comas-Riu, J. and Vives-Rego, J. (2002), Cytometric monitoring of growth, sporogenesis and spore cell
912 sorting in *Paenibacillus polymyxa* (formerly *Bacillus polymyxa*). *Journal of Applied Microbiology*, 92:
913 475-481. doi:10.1046/j.1365-2672.2002.01549.x
- 914 Crawford, I., Robinson, N. H., Flynn, M. J., Foot, V. E., Gallagher, M. W., Huffman, J. A., Stanley, W.
915 R., and Kaye, P. H.: Characterization of bioaerosol emissions from a Colorado pine forest: results from

- 916 the BEACHON-RoMBAS experiment, *Atmospheric Chemistry and Physics Discussions*, 14, 2499-2552,
917 10.5194/acpd-14-2499-2014, 2014.
- 918 Darrow, L. A., Hess, J., Rogers, C. A., Tolbert, P. E., Klein, M., and Sarnat, S. E.: Ambient pollen
919 concentrations and emergency department visits for asthma and wheeze, *Journal of Allergy and Clinical*
920 *Immunology*, 130, 630-638.e634, <https://doi.org/10.1016/j.jaci.2012.06.020>, 2012.
- 921 DeLeon-Rodriguez, N., Terry L. Lathem, Luis M. Rodriguez-R, James M. Barazesh, Bruce E. Anderson,
922 Andreas J. Beyersdorf, Luke D. Ziemba, Michael Bergin, Athanasios Nenes, and Konstantinos T.
923 Konstantinidis.: Microbiome of the upper troposphere: Species composition and prevalence, effects of
924 tropical storms, and atmospheric implications, *Proceedings of the National Academy of Sciences* 110,
925 2575-2580, 2013.
- 926 DeLeon-Rodriguez, N.: Microbes in the atmosphere: prevalence, species composition, and relevance to
927 cloud formation School of Biology Georgia Institute of Technology, 129 pp.,
928 (<http://hdl.handle.net/1853/55517>), 2015.
- 929 Delort, A.-M., and Amato, P.: *Microbiology of aerosols*, pp.167-168, 2018.
- 930 Després, V. R., Alex Huffman, J., Burrows, S. M., Hoose, C., Safatov, A. S., Buryak, G., Fröhlich-
931 Nowoisky, J., Elbert, W., Andreae, M. O., Pöschl, U., and Jaenicke, R.: Primary biological aerosol
932 particles in the atmosphere: a review, *Tellus B*, 64, 10.3402/tellusb.v64i0.15598, 2012.
- 933 Díaz, M., Herrero, M., García, L. A., and Quirós, C.: Application of flow cytometry to industrial
934 microbial bioprocesses, *Biochemical Engineering Journal*, 48, 385-407,
935 <https://doi.org/10.1016/j.bej.2009.07.013>, 2010.
- 936 Eckenrode, H. M., Jen, S.-H., Han, J., Yeh, A.-G., and Dai, H.-L.: Adsorption of a Cationic Dye Molecule
937 on Polystyrene Microspheres in Colloids: Effect of Surface Charge and Composition Probed by Second
938 Harmonic Generation, *The Journal of Physical Chemistry B*, 109, 4646-4653, 10.1021/jp045610q, 2005.
- 939 Elbert, W., Taylor, P. E., Andreae, M. O., & Pöschl, U.: Contribution of fungi to primary biogenic
940 aerosols in the atmosphere: wet and dry discharged spores, carbohydrates, and inorganic ions.,
941 *Atmospheric Chemistry and Physics*, 7, 4569-4588, 2007.
- 942 Fröhlich-Nowoisky, J., Kampf, C. J., Weber, B., Huffman, J. A., Pöhlker, C., Andreae, M. O., Lang-
943 Yona, N., Burrows, S. M., Gunthe, S. S., Elbert, W., Su, H., Hoor, P., Thines, E., Hoffmann, T., Després,
944 V. R., and Pöschl, U.: Bioaerosols in the Earth system: Climate, health, and ecosystem interactions,
945 *Atmospheric Research*, 182, 346-376, <http://dx.doi.org/10.1016/j.atmosres.2016.07.018>, 2016.
- 946 Gabey, A. M., Gallagher, M. W., Whitehead, J., Dorsey, J. R., Kaye, P. H., and Stanley, W. R.:
947 Measurements and comparison of primary biological aerosol above and below a tropical forest canopy
948 using a dual channel fluorescence spectrometer, *Atmospheric Chemistry and Physics*, 10, 4453-4466,
949 10.5194/acp-10-4453-2010, 2010.
- 950 Gabey, A. M., Stanley, W. R., Gallagher, M. W., and Kaye, P. H.: The fluorescence properties of aerosol
951 larger than 0.8 μm in urban and tropical rainforest locations, *Atmospheric Chemistry and Physics*, 11,
952 5491-5504, 10.5194/acp-11-5491-2011, 2011.
- 953 Gosselin, M. I., Rathnayake, C. M., Crawford, I., Pöhlker, C., Fröhlich-Nowoisky, J., Schmer, B.,
954 Després, V. R., Engling, G., Gallagher, M., Stone, E., Pöschl, U., and Huffman, J. A.: Fluorescent

955 bioaerosol particle, molecular tracer, and fungal spore concentrations during dry and rainy periods in a
956 semi-arid forest, *Atmos. Chem. Phys.*, 16, 15165-15184, 10.5194/acp-16-15165-2016, 2016.

957 Goudie, A. S.: Desert dust and human health disorders, *Environment International*, 63, 101-113,
958 <http://dx.doi.org/10.1016/j.envint.2013.10.011>, 2014.

959 Griffin, D. W., Kellogg, C. A., Garrison, V. H., Lisle, J. T., Borden, T. C., and Shinn, E. A.: Atmospheric
960 microbiology in the northern Caribbean during African dust events, *Aerobiologia*, 19, 143-157,
961 10.1023/B:AERO.0000006530.32845.8d, 2003.

962 Grote, M., Valenta, R., and Reichelt, R.: Abortive pollen germination: A mechanism of allergen release in
963 birch, alder, and hazel revealed by immunogold electron microscopy, *J. Allergy Clin. Immun.*, 111, 1017-
964 1023, doi:10.1067/mai.2003.1452, 2003.

965 Guarín, F. A., Abril, M. A. Q., Alvarez, A., and Fonnegra, R.: Atmospheric pollen and spore content in
966 the urban area of the city of Medellin, Colombia, *Hoehnea*, 42, 9-19, 2015.

967 Guindulain, T., J. Comas, and J. Vives-Rego: Use of nucleic acid dyes SYTO-13, TOTO-1, and YOYO-1
968 in the study of *Escherichia coli* and marine prokaryotic populations by flow cytometry, *Applied and*
969 *environmental microbiology*, 63, 4608 - 4611, 1997.

970 Harrison, R. M., Jones, A. M., Biggins, P. D. E., Pomeroy, N., Cox, C. S., Kidd, S. P., Hobman, J. L.,
971 Brown, N. L., and Beswick, A.: Climate factors influencing bacterial count in background air samples,
972 *International Journal of Biometeorology*, 49, 167-178, 10.1007/s00484-004-0225-3, 2005.

973 Healy, D. A., Huffman, J. A., O'Connor, D. J., Pöhlker, C., Pöschl, U., and Sodeau, J. R.: Ambient
974 measurements of biological aerosol particles near Killarney, Ireland: a comparison between real-time
975 fluorescence and microscopy techniques, *Atmos. Chem. Phys.*, 14, 8055-8069, 10.5194/acp-14-8055-
976 2014, 2014.

977 Healy, D. A., O'Connor, D. J., and Sodeau, J. R.: Measurement of the particle counting efficiency of the
978 "Waveband Integrated Bioaerosol Sensor" model number 4 (WIBS-4), *Journal of Aerosol Science*, 47,
979 94-99, <http://dx.doi.org/10.1016/j.jaerosci.2012.01.003>, 2012.

980 Hernandez, M., Perring, A. E., McCabe, K., Kok, G., Granger, G., and Baumgardner, D.: Chamber
981 catalogues of optical and fluorescent signatures distinguish bioaerosol classes, *Atmos. Meas. Tech.*, 9,
982 3283-3292, <https://doi.org/10.5194/amt-9-3283-2016>, 2016.

983 Hill, S. C., Mayo, M. W., and Chang, R. K.: Fluorescence of bacteria, pollens, and naturally occurring
984 airborne particles: excitation/emission spectra, Army Research Lab Adelphi Md Computational And
985 Information Sciences Directorate, 2009.

986 Hoose, C., Kristjánsson, J. E., and Burrows, S. M.: How important is biological ice nucleation in clouds
987 on a global scale?, *Environmental Research Letters*, 5, 024009, 2010.

988 Hoose, C., and Möhler, O.: Heterogeneous ice nucleation on atmospheric aerosols: a review of results
989 from laboratory experiments, *Atmos. Chem. Phys.*, 12, 9817-9854, 10.5194/acp-12-9817-2012, 2012.

990 Huffman, J. A., B. Treutlein, and U. Pöschl: Fluorescent biological aerosol particle concentrations and
991 size distributions measured with an Ultraviolet Aerodynamic Particle Sizer (UV-APS) in Central Europe,
992 *Atmospheric Chemistry and Physics*, 10, 3215-3233, 2010.

- 993 Huffman, J. A., Prenni, A. J., DeMott, P. J., Pöhlker, C., Mason, R. H., Robinson, N. H., Fröhlich-
 994 Nowoisky, J., Tobo, Y., Després, V. R., Garcia, E., Gochis, D. J., Harris, E., Müller-Germann, I., Ruzene,
 995 C., Schmer, B., Sinha, B., Day, D. A., Andreae, M. O., Jimenez, J. L., Gallagher, M., Kreidenweis, S. M.,
 996 Bertram, A. K., and Pöschl, U.: High concentrations of biological aerosol particles and ice nuclei during
 997 and after rain, *Atmospheric Chemistry and Physics*, 13, 6151-6164, 10.5194/acp-13-6151-2013, 2013.
- 998 Ingold, C. T.: Fungal spores. Their liberation and dispersal, Oxford, Clarendon Press., 302 pp. pp., 1971.
- 999 Joly, M., Amato, P., Sancelme, M., Vinatier, V., Abrantes, M., Deguillaume, L., and Delort, A.-M.:
 1000 Survival of microbial isolates from clouds toward simulated atmospheric stress factors, *Atmospheric*
 1001 *Environment*, 117, 92-98, <https://doi.org/10.1016/j.atmosenv.2015.07.009>, 2015.
- 1002 Joung, Y. S., and Buie, C. R.: Aerosol generation by raindrop impact on soil, 6, 6083,
 1003 10.1038/ncomms7083, <https://www.nature.com/articles/ncomms7083#supplementary-information>, 2015.
- 1004 Kesavan, J., and Sagripanti, J. L.: Evaluation criteria for bioaerosol samplers, *Environ Sci Process*
 1005 *Impacts*, 17, 638-645, 10.1039/c4em00510d, 2015.
- 1006 Lange, J. L. T., P S and Lynch, N: Application of flow cytometry and fluorescent in situ hybridization for
 1007 assessment of exposures to airborne bacteria *Appl. Environ. Microbiol.* , 63, 1557-1563, 1997.
- 1008 Lebaron, P., Servais, P., Agogue, H., Courties, C., and Joux, F.: Does the high nucleic acid content of
 1009 individual bacterial cells allow us to discriminate between active cells and inactive cells in aquatic
 1010 systems?, *Appl Environ Microbiol*, 67, 1775-1782, 10.1128/AEM.67.4.1775-1782.2001, 2001.
- 1011 Li, D.-W., and Bryce Kendrick: A year-round study on functional relationships of airborne fungi with
 1012 meteorological factors, *International Journal of Biometeorology* 39, 74-80, 1995.
- 1013 Liang, L., Engling, G., Cheng, Y., Duan, F., Du, Z., and He, K.: Rapid detection and quantification of
 1014 fungal spores in the urban atmosphere by flow cytometry, *Journal of Aerosol Science*, 66, 179-186,
 1015 10.1016/j.jaerosci.2013.08.013, 2013.
- 1016 Lin, H., Gomez, I., and Meredith, J. C.: Pollenkit Wetting Mechanism Enables Species-Specific Tunable
 1017 Pollen Adhesion, *Langmuir*, 29, 3012-3023, 10.1021/la305144z, 2013.
- 1018 Longo, A. F., Ingall, E. D., Diaz, J. M., Oakes, M., King, L. E., Nenes, A., Mihalopoulos, N., Violaki, K.,
 1019 Avila, A., Benitez-Nelson, C. R., Brandes, J., McNulty, I., and Vine, D. J.: P-NEXFS analysis of aerosol
 1020 phosphorus delivered to the Mediterranean Sea, *Geophysical Research Letters*, 41, 4043-4049,
 1021 10.1002/2014GL060555, 2014.
- 1022 Mage, P. L., Csordas, A. T., Brown, T., Klinger, D., Eisenstein, M., Mitragotri, S., Hawker, C., and Soh,
 1023 H. T.: Shape-based separation of synthetic microparticles, *Nature materials*, 18, 82, 2019.
- 1024 Mathaes, R., Winter, G., Engert, J., and Besheer, A.: Application of different analytical methods for the
 1025 characterization of non-spherical micro- and nanoparticles, *International journal of pharmaceutics*, 453,
 1026 620-629, 2013.
- 1027 Monier, J. M., and Lindow, S. E.: *Pseudomonas syringae* Responds to the Environment on Leaves by Cell
 1028 Size Reduction, *Phytopathology*, 93, 1209-1216, 10.1094/PHYTO.2003.93.10.1209, 2003.

- 1029 Morris, C. E., Conen, F., Alex Huffman, J., Phillips, V., Poschl, U., and Sands, D. C.: Bioprecipitation: a
 1030 feedback cycle linking earth history, ecosystem dynamics and land use through biological ice nucleators
 1031 in the atmosphere, *Glob Chang Biol*, 20, 341-351, 10.1111/gcb.12447, 2014.
- 1032 Muller, S., and Nebe-von-Caron, G.: Functional single-cell analyses: flow cytometry and cell sorting of
 1033 microbial populations and communities, *FEMS Microbiol Rev*, 34, 554-587, 10.1111/j.1574-
 1034 6976.2010.00214.x, 2010.
- 1035 Myriokefalitakis, S., Nenes, A., Baker, A. R., Mihalopoulos, N., and Kanakidou, M.: Bioavailable
 1036 atmospheric phosphorous supply to the global ocean: a 3-D global modeling study, *Biogeosciences*, 13,
 1037 6519-6543, 10.5194/bg-13-6519-2016, 2016.
- 1038 Nir, R., Yisraeli, Y., Lamed, R., & Sahar, E.: Flow cytometry sorting of viable bacteria and yeasts
 1039 according to beta-galactosidase activity, *Applied and environmental microbiology*, 56, 3861-3866, 1990.
- 1040 Oliveira, M., Ribeiro, H., Delgado, J. L., and Abreu, I.: The effects of meteorological factors on airborne
 1041 fungal spore concentration in two areas differing in urbanisation level, *Int J Biometeorol*, 53, 61-73,
 1042 10.1007/s00484-008-0191-2, 2009.
- 1043
- 1044 Ortiz-Martínez, Mario G., Rosa I. Rodríguez-Cotto, Mónica A. Ortiz-Rivera, Cedric W. Pluguez-Turull,
 1045 and Braulio D. Jiménez-Vélez. Linking endotoxins, African dust PM10 and asthma in an urban and rural
 1046 environment of Puerto Rico. *Mediators of inflammation* 2015.
- 1047 Pan, Y.-L., Santarpia, J. L., Ratnesar-Shumate, S., Corson, E., Eshbaugh, J., Hill, S. C., Williamson, C. C.,
 1048 Coleman, M., Bare, C., and Kinahan, S.: Effects of ozone and relative humidity on fluorescence spectra of
 1049 octapeptide bioaerosol particles, *Journal of Quantitative Spectroscopy and Radiative Transfer*, 133, 538-
 1050 550, <https://doi.org/10.1016/j.jqsrt.2013.09.017>, 2014.
- 1051 Perring, A. E., et al. (2015), Airborne observations of regional variation in fluorescent aerosol across the
 1052 United States, *J. Geophys. Res. Atmos.*, 120, 1153–1170, doi:10.1002/2014JD022495.
- 1053 Pöhlker, C., Huffman, J. A., Förster, J. D., and Pöschl, U.: Autofluorescence of atmospheric bioaerosols:
 1054 spectral fingerprints and taxonomic trends of pollen, *Atmospheric Measurement Techniques*, 6, 3369-
 1055 3392, 10.5194/amt-6-3369-2013, 2013.
- 1056 Pöhlker, C., Huffman, J. A., and Pöschl, U.: Autofluorescence of atmospheric bioaerosols – fluorescent
 1057 biomolecules and potential interferences, *Atmospheric Measurement Techniques*, 5, 37-71, 10.5194/amt-
 1058 5-37-2012, 2012.
- 1059 Pöschl, U.: Atmospheric Aerosols: Composition, Transformation, Climate and Health Effects,
 1060 *Angewandte Chemie International Edition*, 44, 7520-7540, 10.1002/anie.200501122, 2005.
- 1061 Robinson, N. H., Allan, J. D., Huffman, J. A., Kaye, P. H., Foot, V. E., and Gallagher, M.: Cluster
 1062 analysis of WIBS single-particle bioaerosol data, *Atmos. Meas. Tech.*, 6, 337-347,
 1063 <https://doi.org/10.5194/amt-6-337-2013>, 2013.
- 1064 Rödiger, S., Ruhland, M., Schmidt, C., Schröder, C., Grossmann, K., Böhm, A., Nitschke, J., Berger, I.,
 1065 Schimke, I., and Schierack, P.: Fluorescence Dye Adsorption Assay to Quantify Carboxyl Groups on the
 1066 Surface of Poly(methyl methacrylate) Microbeads, *Analytical Chemistry*, 83, 3379-3385,
 1067 10.1021/ac103277s, 2011.

- 1068 S.-L.Von der Weiden, F. D., and S. Borrmann: Particle Loss Calculator - a new software tool for the
1069 assessment of the performance of aerosol inlet systems, *Atmospheric Measurement Techniques*, 2, 479-
1070 494, 2009.
- 1071 Saari, S., Reponen, T., and Keskinen, J.: Performance of Two Fluorescence-Based Real-Time Bioaerosol
1072 Detectors: BioScout vs. UVAPS, *Aerosol Science and Technology*, 48, 371-378,
1073 10.1080/02786826.2013.877579, 2014.
- 1074 Šantl-Temkiv, T., Amato, P., Gosewinkel, U., Thyrhaug, R., Charton, A., Chicot, B., Finster, K., Bratbak,
1075 G., and Löndahl, J.: High-Flow-Rate Impinger for the Study of Concentration, Viability, Metabolic
1076 Activity, and Ice-Nucleation Activity of Airborne Bacteria, *Environmental Science & Technology*, 51,
1077 11224-11234, 10.1021/acs.est.7b01480, 2017.
- 1078 Savage, N. J., Krentz, C. E., Könemann, T., Han, T. T., Mainelis, G., Pöhlker, C., and Huffman, J. A.:
1079 Systematic characterization and fluorescence threshold strategies for the wideband integrated bioaerosol
1080 sensor (WIBS) using size-resolved biological and interfering particles, *Atmospheric Measurement
1081 Techniques*, 10, 4279-4302, 10.5194/amt-10-4279-2017, 2017.
- 1082 Shapiro, Howard M. *Practical flow cytometry*. John Wiley & Sons, 2005.
- 1083 Standaert-Vitse, A., Aliouat-Denis, C.-M., Martinez, A., Khalife, S., Pottier, M., Gantois, N., Dei-Cas, E.,
1084 and Aliouat, E. M.: SYTO-13, a Viability Marker as a New Tool to Monitor In Vitro Pharmacodynamic
1085 Parameters of Anti-Pneumocystis Drugs, *PLoS One*, 10, e0130358-e0130358,
1086 10.1371/journal.pone.0130358, 2015.
- 1087 Sullivan, S. C., Hoose, C., Kiselev, A., Leisner, T., and Nenes, A.: Initiation of secondary ice production
1088 in clouds, *Atmos. Chem. Phys. Discuss.*, 2017, 1-22, 10.5194/acp-2017-387, 2017.
- 1089 Taylor, P. E., Jacobson, K. W., House, J. M., and Glovsky, M. M.: Links between pollen, atopy and the
1090 asthma epidemic, *Int Arch Allergy Immunol*, 144, 162-170, 10.1159/000103230, 2007.
- 1091 Toprak, E., and Schnaiter, M.: Fluorescent biological aerosol particles measured with the Waveband
1092 Integrated Bioaerosol Sensor WIBS-4: laboratory tests combined with a one year field study,
1093 *Atmospheric Chemistry and Physics*, 13, 225-243, 10.5194/acp-13-225-2013, 2013.
- 1094 Troussellier, M., Courties, C., Lebaron, P., and Servais, P.: Flow cytometric discrimination of bacterial
1095 populations in seawater based on SYTO 13 staining of nucleic acids, *FEMS Microbiology Ecology*, 29,
1096 319-330, [https://doi.org/10.1016/S0168-6496\(99\)00026-4](https://doi.org/10.1016/S0168-6496(99)00026-4), 1999.
- 1097 Tzur A, Moore JK, Jorgensen P, Shapiro HM, Kirschner MW (2011) Optimizing Optical Flow Cytometry
1098 for Cell Volume-Based Sorting and Analysis. *PLoS ONE* 6(1): e16053.
1099 <https://doi.org/10.1371/journal.pone.0016053>
- 1100 Van Dilla, M. A., Langlois, R. G., Pinkel, D., Yajko, D., & Hadley, W. K.: Bacterial characterization by
1101 flow cytometry., *Science*, 220, 620-622, 1983.
- 1102 Wang, Y., Hammes, F., De Roy, K., Verstraete, W., and Boon, N.: Past, present and future applications of
1103 flow cytometry in aquatic microbiology, *Trends Biotechnol*, 28, 416-424, 10.1016/j.tibtech.2010.04.006,
1104 2010.

- 1105 Wu, Y.-H., Chan, C.-C., Rao, C. Y., Lee, C.-T., Hsu, H.-H., Chiu, Y.-H., and Chao, H. J.: Characteristics,
1106 determinants, and spatial variations of ambient fungal levels in the subtropical Taipei metropolis,
1107 *Atmospheric Environment*, 41, 2500-2509, 10.1016/j.atmosenv.2006.11.035, 2007.
- 1108 Yu, X., Wang, Z., Zhang, M., Kuhn, U., Xie, Z., Cheng, Y., Pöschl, U., and Su, H.: Ambient
1109 measurement of fluorescent aerosol particles with a WIBS in the
- 1110 Yangtze River Delta of China: potential impacts of combustion-related aerosol particles, *Atmospheric*
1111 *Chemistry and Physics*, 16, 11337-11348, 10.5194/acp-16-11337-2016, 2016.
- 1112 Yue, S., Ren, H., Fan, S., Sun, Y., Wang, Z., and Fu, P.: Springtime precipitation effects on the
1113 abundance of fluorescent biological aerosol particles and HULIS in Beijing, *Sci Rep*, 6, 29618,
1114 10.1038/srep29618, 2016.
- 1115 Yue, S., Ren, H., Fan, S., Wei, L., Zhao, J., Bao, M., Hou, S., Zhan, J., Zhao, W., Ren, L., Kang, M., Li,
1116 L., Zhang, Y., Sun, Y., Wang, Z., and Fu, P.: High Abundance of Fluorescent Biological Aerosol
1117 Particles in Winter in Beijing, China, *ACS Earth and Space Chemistry*, 1, 493-502,
1118 10.1021/acsearthspacechem.7b00062, 2017.
- 1119 Zhen, H., Han, T., Fennell, D. E., and Mainelis, G.: Release of free DNA by membrane-impaired bacterial
1120 aerosols due to aerosolization and air sampling, *Appl Environ Microbiol*, 79, 7780-7789,
1121 10.1128/AEM.02859-13, 2013.
- 1122 Ziemba, L. D., Beyersdorf, A. J., Chen, G., Corr, C. A., Crumeyrolle, S. N., Diskin, G., Hudgins, C.,
1123 Martin, R., Mikoviny, T., Moore, R., Shook, M., Thornhill, K. L., Winstead, E. L., Wisthaler, A., and
1124 Anderson, B. E.: Airborne observations of bioaerosol over the Southeast United States using a Wideband
1125 Integrated Bioaerosol Sensor, *Journal of Geophysical Research: Atmospheres*, 121, 8506-8524,
1126 10.1002/2015JD024669, 2016.
- 1127

1 **Table 1:** Summary of the SpinCon II sampling events, the 24 h. averaged RH, ambient temperature, the
 2 assigned meteorological category (using Section 4.4 definitions) and the corrected FCM-derived PBAP
 3 number concentration (1 to 5 μm) for each sample collected during this study.

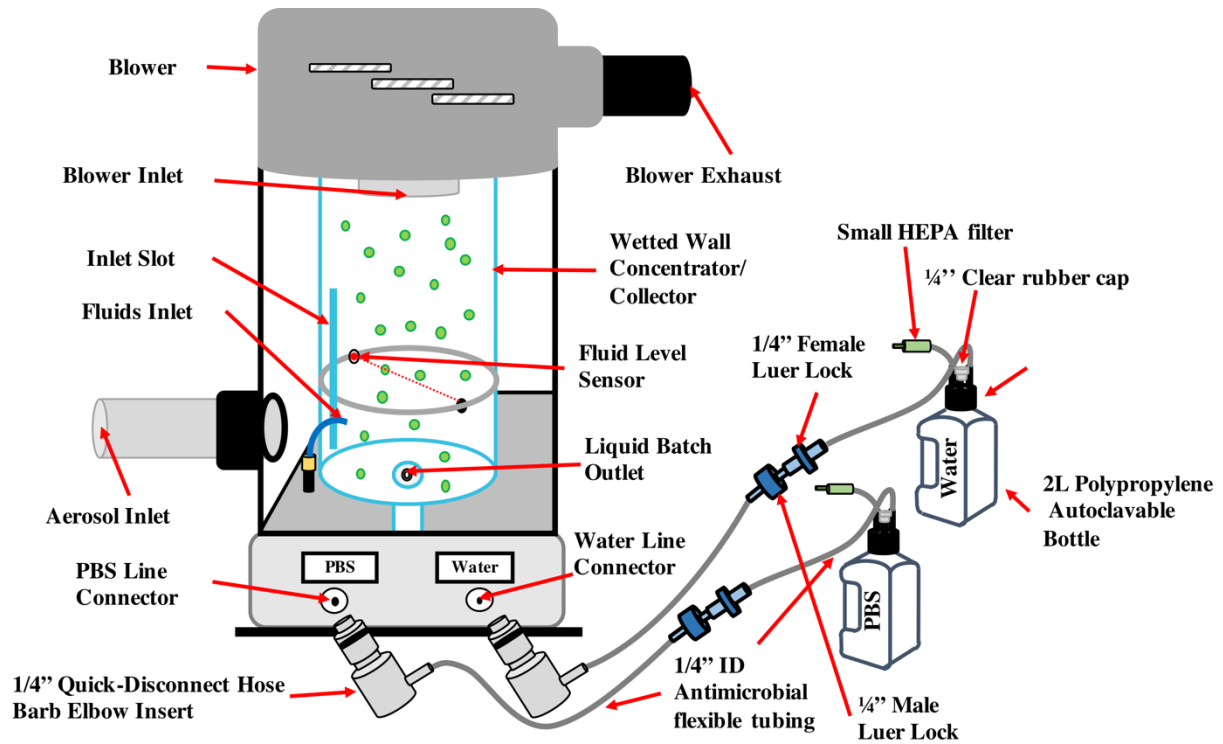
4

Date (starting – ending time)	RH (%)	Temperature (°C)	Meteorological Category	PBAP Concentration (m^{-3}) 1 to 5μm diameter range
4/7/15 (11:17 - 15:17) *	70.9	21.4	Humid, Warm	9.282×10^4
4/8/15 (11:10 - 15:10)	53.6	24.9	Dry, Warm	5.203×10^5
4/9/15 (11:15 - 15:15)	53.8	25.3	Dry, Warm	1.254×10^5
4/14/15 (11:30 - 15:30) *	76.8	22.5	Humid, Warm	8.253×10^4
4/15/15 (11:40 - 15:40) *	83.6	18.9	Humid, Warm	1.234×10^5
4/16/15 (10:55 - 14:55)	86.3	12.5	Humid, Cold	3.399×10^5
4/21/15 (13:15 - 17:15)	43.2	16.6	Dry, Cold	4.741×10^5
4/22/15 (11:25 - 15:25)	38.1	18.8	Dry, Warm	3.351×10^5
4/23/15 (11:35 - 15:35)	48.1	16.8	Dry, Cold	1.708×10^6
4/28/15 (12:25 - 16:25)	45.3	17.0	Dry, Cold	4.899×10^5
4/29/15 (11:55 - 15:55) #	79.4	14.2	Humid, Cold	4.591×10^5
4/30/15 (12:10 - 16:10)	57.3	17.4	Dry, Cold	9.603×10^5
5/13/15 (10:50 - 14:50)	40.1	23.5	Dry, Warm	3.680×10^5
5/14/15 (11:50 - 15:50)	52.3	23.0	Dry, Warm	4.851×10^5
5/15/15 (10:19 - 14:19)	64.4	23.1	Dry, Warm	1.656×10^6

5 * Sampling occurred post-rain event.

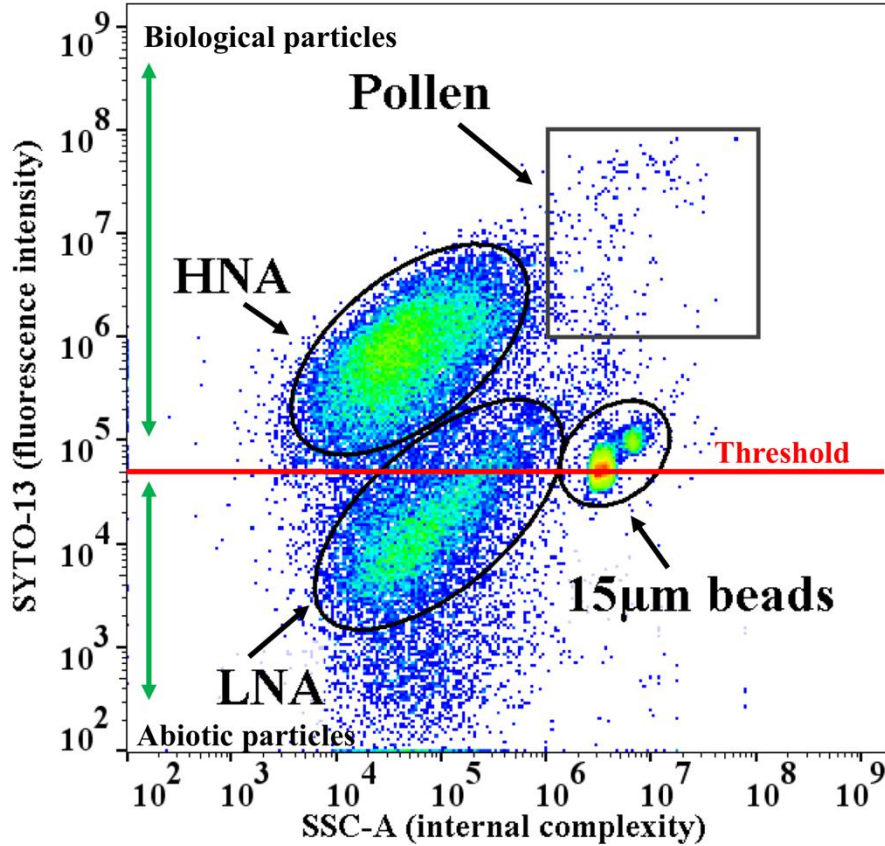
6 # Sampling occurred during a rain event.

7



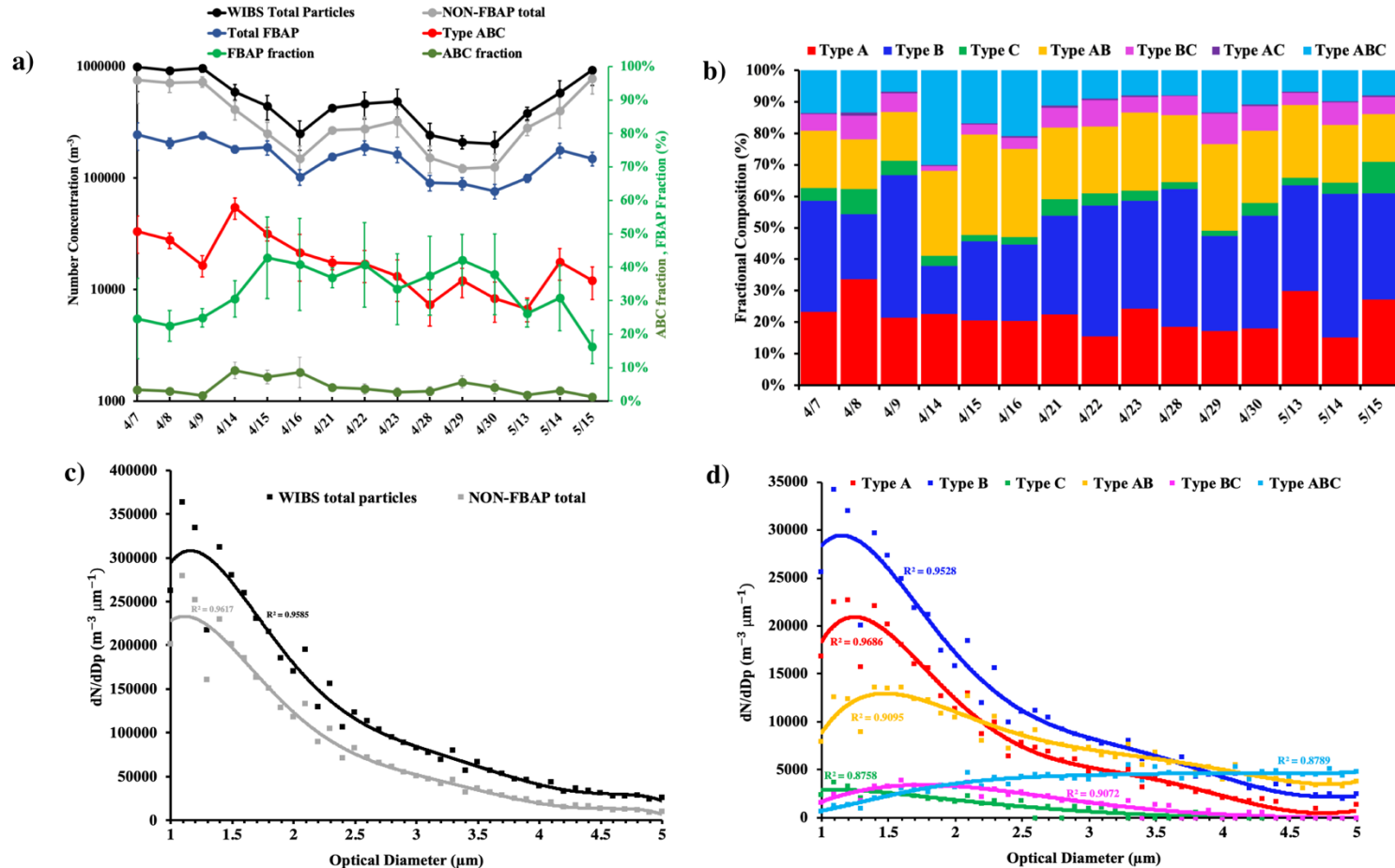
8
9
10

Figure 1: SpinCon II sampling setup including modified fluid supply system with anti-microbial tubing and 2L Autoclavable bottles.



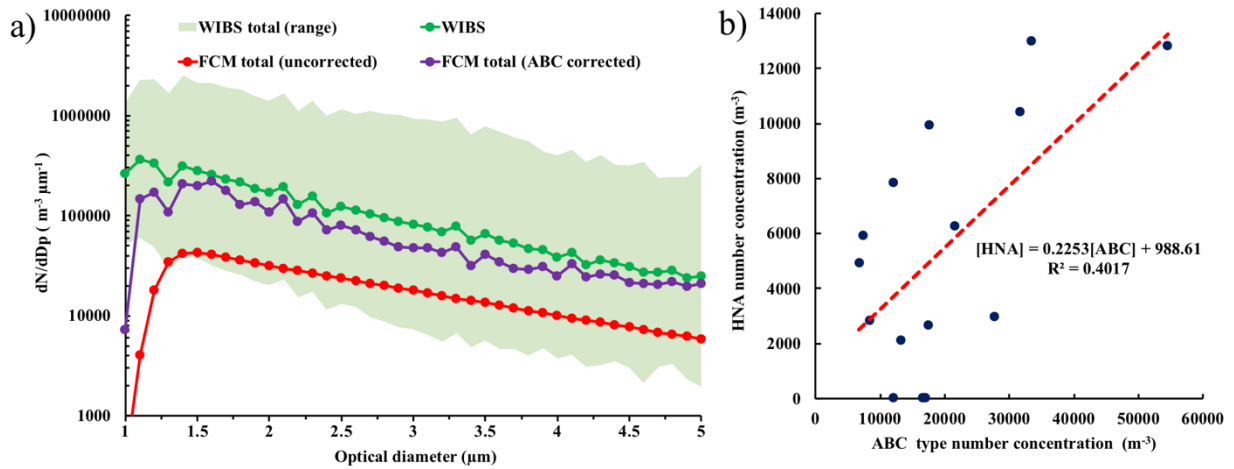
11
 12
 13
 14
 15
 16
 17
 18
 19
 20

Figure 2: FL1-A vs. SSC-A plot used to identify populations in the April 14, 2015 sample including: the 42k threshold line in red and, abiotic particles (below threshold) and biological particles (above threshold) designated regions. In the density plot green and red zones denote the most populated regions. FL1-A in the y-axis shows the fluorescence intensity of each particle in the plot stained with SYTO-13 and SSC-A in the x-axis measures 90° light scattering, related to the internal complexity (e.g. granularity or amount of internal structures) of the particles. The fraction of the LNA population above the threshold line is referred as the “LNA-AT” population.



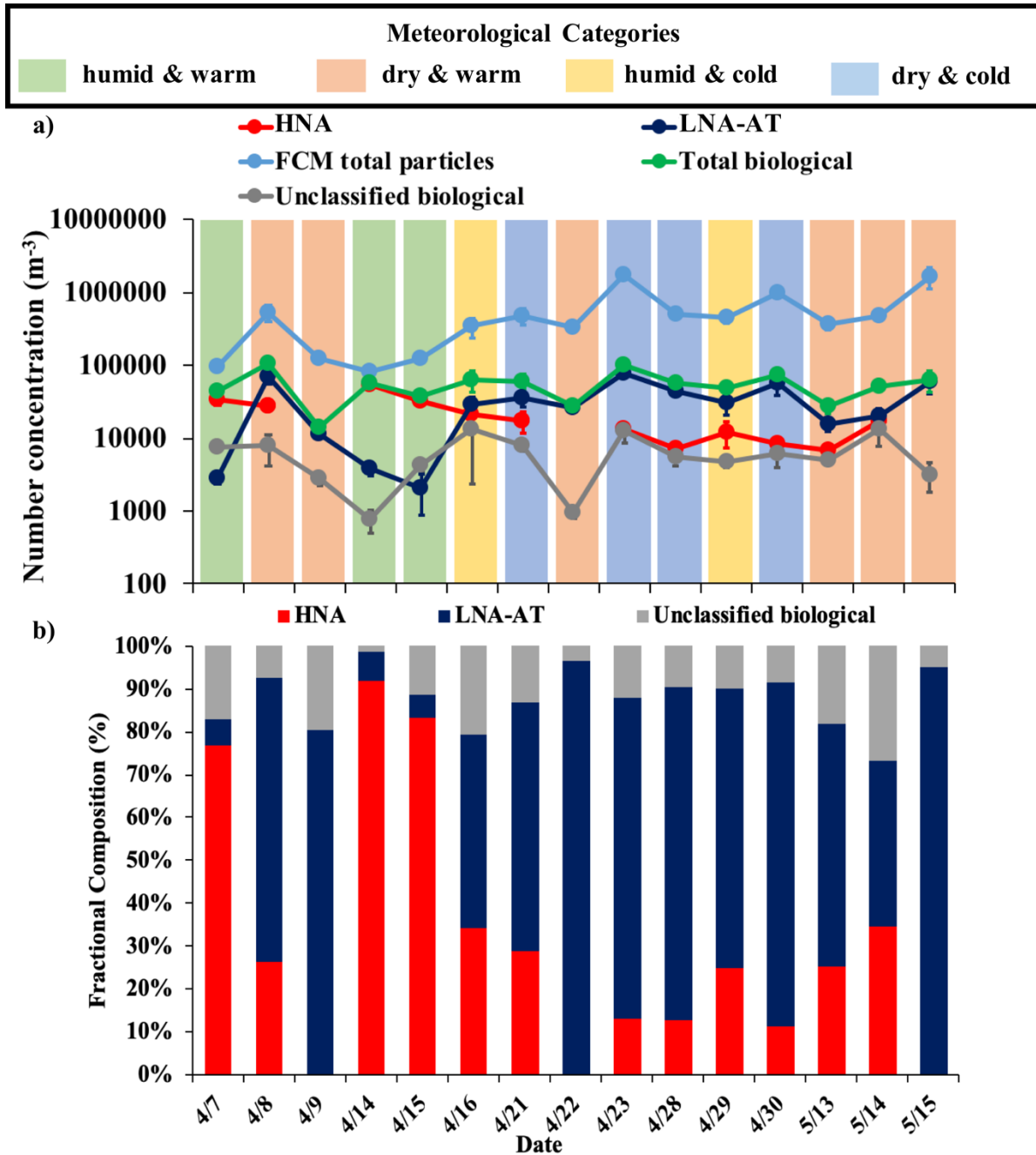
21

22 **Figure 3:** WBS-4A 4hr (SpinCon II sampling time) averaged results of WBS total particle, NON-FBAP, total FBAP and type ABC
 23 concentrations in the left Y-axis and ABC and FBAP fraction in the right Y-axis for each SpinCon II sampling event in (a); 4hr averaged FBAP
 24 types number concentration fractional composition for each SpinCon II sampling event in (b); 1to5 μm WBS total particles and NON-FBAP size
 25 distributions in (c) and 1to5 μm size distributions for all FBAP types, except AC type in (d). AC type showed low statistics and constituted less
 26 than 1% of the total FBAP (not shown). Size distributions in (c) and (d) have been averaged over the 15 SpinCon II sampling events and constitute
 27 the overall size distributions during rooftop sampling events. Solid lines in (c) and (d) shown 6-degree polynomial regressions performed to FBAP
 28 the size distributions, including their respective correlation coefficients (R^2).



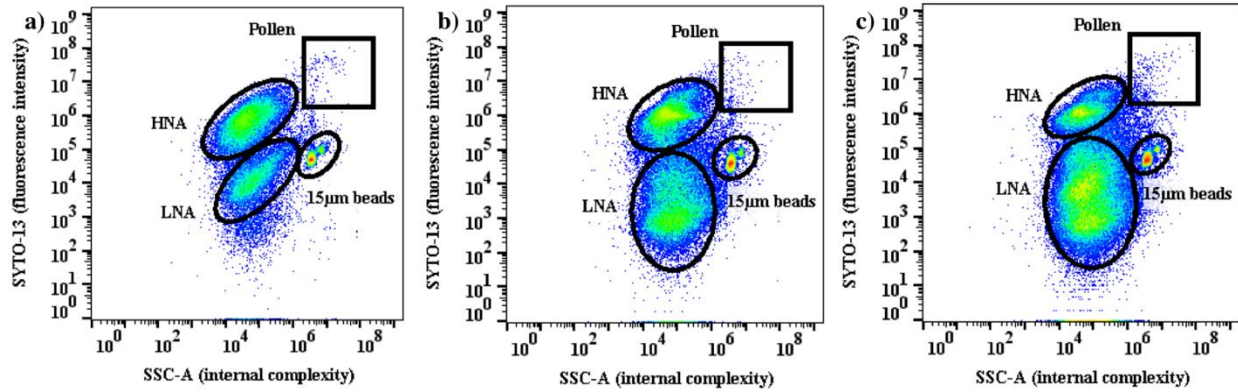
29
 30 **Figure 4:** WIBS-4A, FCM uncorrected and FCM (ABC corrected) total particle concentration (1 to 5 μ m)
 31 average size distributions (geometrically averaged over the 15 SpinCon II sampling events) including WIBS
 32 range (\pm geometric standard deviation factor) in (a); and HNA and ABC type concentration correlation in
 33 the 1 to 5 μ m range in (b) including its linear correlation in red.

34
 35



37
38
39
40
41
42
43
44
45
46
47

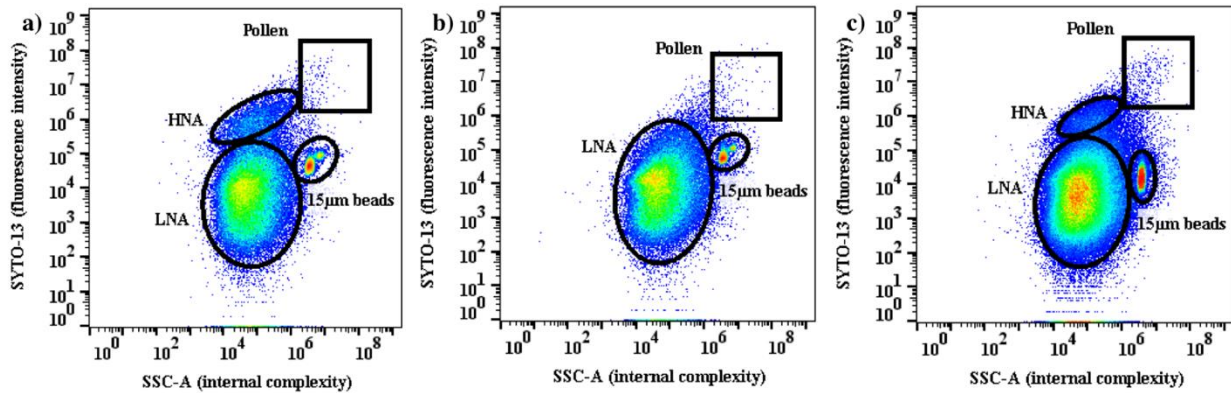
Figure 5: FCM total particle, HNA, LNA-AT and total PBAP number concentrations in the 1 to 5 μ m range highlighting the prevailing meteorological category during each sampling event in (a); HNA and LNA-AT number concentration fractional compositions for each sampling event in (b).



48
49
50
51
52
53
54

55
56
57

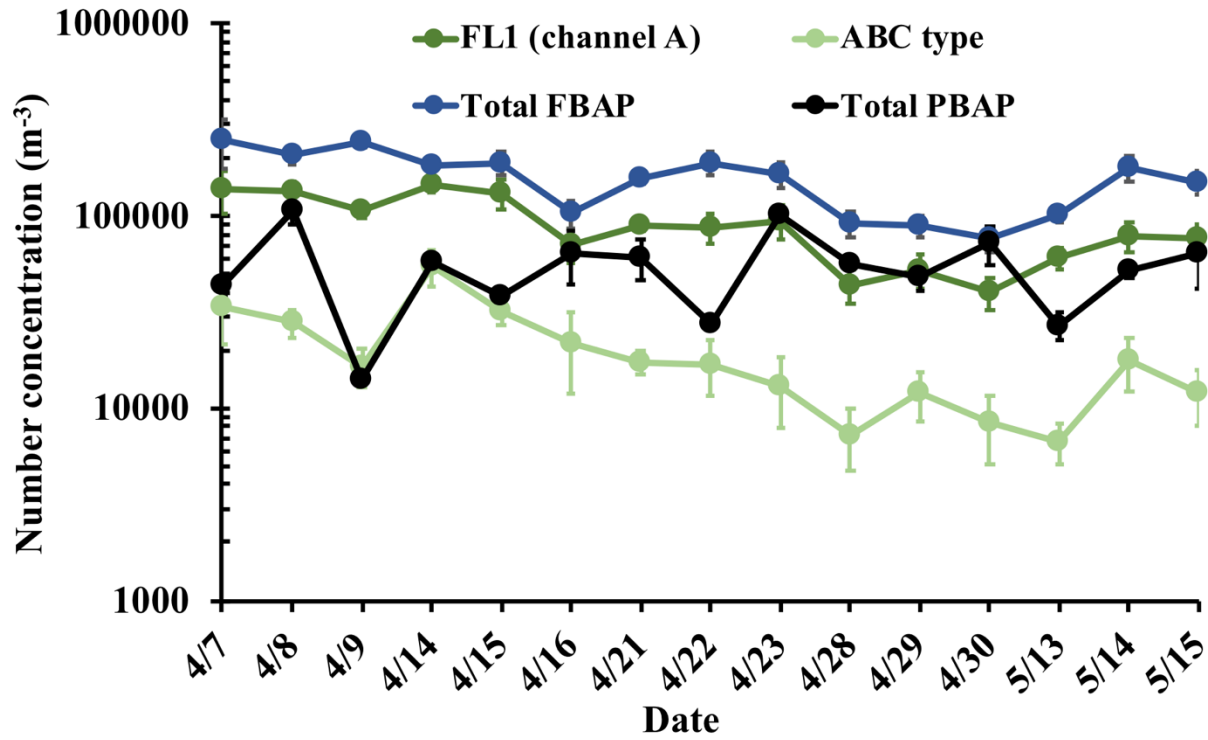
Figure 6: FL1-A vs. SSC-A FSC plots for (a) April 14, (b) April 15, and (c) April 16. This period was characterized by a transition from humid & warm to humid & cold conditions (diurnal average RH=77%, T=22.5 °C on 4/14; RH=84%, T=18.9 °C on 4/15, and RH= 86%, T= 12.5 °C on 4/16). The FCM plots during this transition period show a decrease of fungal population and an increase of the LNA population. In each population, warmer colors represent higher particle concentrations.



58
59
60
61
62
63

64
65
66
67
68
69
70
71
72
73

Figure 7: Similar to Figure 6, but for (a) April 21, (b) April 22, (c) April 23, which was characterized by dry and variability in temperature (diurnal average RH=43%, T=16.6 °C on 4/21; RH=41%, T=19.0 °C on 4/22, and, RH= 48%, T= 16.8 °C on 4/23). Note the disappearance of the fungal spore population on the warmest day (4/22).



74

75 **Figure 8:** WIBS-4A total FBAP, FL1 and ABC type, and FCM total particle number concentrations in
 76 the 1 to 5 μ m range for each sampling event from April 7 to May 15, 2015.

77

78

79

80

81

82

83

84

85